Published in final edited form as:

Free Radic Biol Med. 2015 December ; 89: 1231–1247. doi:10.1016/j.freeradbiomed.2015.10.416.

Anticancer therapeutic potential of Mn porphyrin/ascorbate system

Artak Tovmasyan[1], **Romulo S. Sampaio**[1,2], **Mary-Keara Boss**[3], **Jacqueline C. Bueno-Janice**[1,2], **Bader H. Bader**[4], **Milini Thomas**[4], **Julio S. Reboucas**[2], **Michael Orr**[5], **Joshua D. Chandler**[5], **Young-Mi Go**[5], **Dean P. Jones**[5], **Talaignair N. Venkatraman**[6], **Sinisa Haberle**[6,#], **Natalia Kyui**[7], **Christopher Lascola**[6], **Mark W. Dewhirst**[1], **Ivan Spasojevic**[8,9], **Ludmil Benov**[4], and **Ines Batinic-Haberle**[1,*]

[1]Department of Radiation Oncology, Duke University School of Medicine, Durham, NC 27710

[2]Departamento de Quimica, CCEN, Universidade Federal da Paraiba, Joao Pessoa, PB 58051-900, Brazil

[3]Department of Molecular Biomedical Sciences, North Carolina State University College of Veterinary Medicine, Raleigh, NC 27607

[4]Department of Biochemistry, Faculty of Medicine, Kuwait University, Kuwait

[5]Division of Pulmonary, Allergy and Critical Care Medicine, Department of Medicine, Emory University, Atlanta, Georgia

[6]Department of Radiology, Duke University School of Medicine, Durham, NC 27710

[7]Canadian Economic Analysis Department, Bank of Canada, Ottawa, Ontario, Canada K1A 0G9

[8]Department of Medicine, Duke University School of Medicine, Durham, NC 27710

[9]Duke Cancer Institute, Pharmaceutical Research Shared Resource, PK/PD Core laboratory, Durham NC 27710

Abstract

Ascorbate (Asc) as a single agent suppressed growth of several tumor cell lines in a mouse model. It has been tested in a Phase I Clinical Trial on pancreatic cancer patients where it exhibited no toxicity to normal tissue yet was of only marginal efficacy. The mechanism of its anticancer effect was attributed to the production of tumoricidal hydrogen peroxide (H_2O_2) during ascorbate oxidation catalyzed by endogenous metalloproteins. The amount of H_2O_2 could be maximized with exogenous catalyst that has optimized properties for such function and is localized within tumor. Herein we studied 14 Mn porphyrins (MnPs) which differ vastly with regards to their redox

[*]*corresponding author*, ***Ines Batinic-Haberle***, Duke University School of Medicine, Research Dr., MSRBI, 281b/285, Durham, NC 27710, Tel: 919-684-2101, Fax: 919-684-8718, ibatinic@duke.edu.

[#]*present address* Cincinnati Children's Hospital Medical Center, Department of Radiology – MLC 5031, 3333 Burnet Avenue, Cincinnati, OH 45229-3026

properties, charge, size/bulkiness and lipophilicity. Such properties affect the *in vitro* and *in vivo* ability of MnPs **(i)** to catalyze ascorbate oxidation resulting in the production of H_2O_2; **(ii)** to subsequently employ H_2O_2 in the catalysis of signaling proteins oxidations affecting cellular survival pathways; and **(iii)** to accumulate at site(s) of interest. The metal-centered reduction potential of MnPs studied, $E_{1/2}$ of $Mn^{III}P/Mn^{II}P$ redox couple, ranged from −200 to +350 mV *vs* NHE. Anionic and cationic, hydrophilic and lipophilic as well as short- and long-chained and bulky compounds were explored. Their ability to catalyze ascorbate oxidation, and in turn cytotoxic H_2O_2 production, was explored *via* spectrophotometric and electrochemical means. Bell-shape structure-activity relationship (SAR) was found between the initial rate for the catalysis of ascorbate oxidation, $v_o(Asc)_{ox}$ and $E_{1/2}$, identifying cationic Mn(III) *N*-substituted pyridylporphyrins with $E_{1/2} > 0$ mV *vs* NHE as efficient catalysts for ascorbate oxidation. The anticancer potential of MnPs/Asc system was subsequently tested in cellular (human MCF-7, MDA-MB-231 and mouse 4T1) and animal models of breast cancer. At the concentrations where ascorbate (1 mM) and MnPs (1 or 5 μM) alone did not trigger any alteration in cell viability, combined treatment suppressed cell viability up to 95%. No toxicity was observed with normal human breast epithelial HBL100 cells. Bell-shape relationship, essentially identical to $v_o(Asc)_{ox}$ *vs* $E_{1/2}$, was also demonstrated between MnP/Asc-controlled cellular cytotoxicity and $E_{1/2}$-controlled $v_o(Asc)_{ox}$. Magnetic resonance imaging studies were conducted to explore the impact of ascorbate on T1-relaxivity. The impact of MnP/Asc on intracellular thiols and on GSH/GSSG and Cys/CySS ratios in 4T1 cells was assessed and cellular reduction potentials were calculated. The data indicate a significant increase in cellular oxidative stress induced by MnP/Asc. Based on $v_o(Asc)_{ox}$ *vs* $E_{1/2}$ relationships and cellular cytotoxicity, MnTE-2-PyP^{5+} was identified as the best catalyst among MnPs studied. Asc and MnTE-2-PyP^{5+} were thus tested in a 4T1 mammary mouse flank tumor model. The combination of ascorbate (4 g/kg) and MnTE-2-PyP^{5+} (0.2 mg/kg) showed significant suppression of tumor growth relative to either MnTE-2-PyP^{5+} or ascorbate alone. In addition to optimal $v_o(Asc)_{ox}$, the compound must be also bioavailable at the site of interest. About 7-fold higher accumulation of MnTE-2-PyP^{5+} in tumor *vs* normal tissue was found to contribute largely to the anticancer effect.

Graphical Abstract

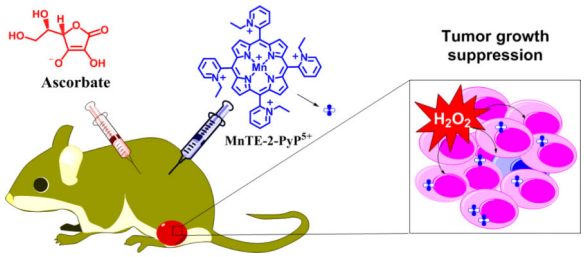

INTRODUCTION

Cationic Mn(III) *N*-substituted pyridyl-porphyrins (MnPs) bear large therapeutic potential as tumor radio- and chemosensitizers, while radioprotectors of normal tissue [1-7]. The anticancer and radioprotective effects, demonstrated in numerous *in vitro* and *in vivo* studies, have been reported and the related mechanism(s) discussed elsewhere [1-9]. A lead

compound, Mn(III) *meso*-tetrakis(*N*-butoxyethylpyridinium-2-yl)porphyrin, MnTnBuOE-2-PyP^{5+} (BMX-001) is entering Phase I/II Clinical Trials at Duke University as a radioprotector of normal tissue in head and neck, and glioma cancer patients. Differential effects in tumor *vs* normal tissue arise predominantly from their differential redox environments [10, 11]. The levels of reactive species (RS) are present at much higher levels in tumor than in normal tissue [12-14]. Differential levels of RS are at least in part due to the differential expression and/or activities of endogenous antioxidant defenses such as superoxide dismutases (SOD), glutathione peroxidases (GPx), catalase and peroxiredoxins [8, 9, 15-31]. Substantial evidence was provided that MnPs are involved in the production of H_2O_2; moreover MnP uses H_2O_2 along with GSH in the catalysis of *S*-glutathionylation of signaling proteins in either thiol-oxidase or GPx-like fashion [10, 11, 32, 33]. Subsequently, the activities of those signaling proteins get suppressed; the magnitude of the effect controls cell survival. The impact of MnPs on master transcription factor, NF-κB has most frequently been assessed [8-11, 21, 34-37].

Similar to radiation and chemotherapy, metal-catalyzed ascorbate oxidation is another means to inhibit tumor growth via excessive H_2O_2 production. Thus exogenous, pharmacologic ascorbate was tested as a single agent in a Phase I Clinical Trial on pancreatic cancer patients [38]. While no safety concerns were raised, only marginal anticancer effect was demonstrated [38]. The ascorbate oxidation was catalyzed by endogenous metalloproteins, presumably metal-containing porphyrins such as *cyt* P450 family of enzymes [39-41]. We have already indicated that cationic MnPs may be better catalysts for ascorbate oxidation than endogenous metalloproteins [33, 42-45]. Others subsequently confirmed that MnP-driven catalysis of ascorbate oxidation bears anticancer therapeutic potential [39, 46-49]. Our studies have thus far aimed at identifying those properties of MnPs which are critical for their *in vivo* anticancer therapeutic potential: **(i)** ability to catalyze ascorbate oxidation; **(ii)** ability to employ H_2O_2 in a subsequent catalysis of oxidation or *S*-glutathionylation of thiols, and **(iii)** bioavailability in the close vicinity or at the site of interest. Understanding the mechanism behind the effects induced by MnP/Asc system as a source of H_2O_2, will be relevant to coupling of MnP with any source of H_2O_2, including radiation and chemotherapy. It has to be pointed out that ascorbate is our major endogenous reductant. Thus, even if it is not added exogenously, MnP would couple with endogenous ascorbate, yet with a lower yield of H_2O_2 production. Different aspects of the role of ascorbate in MnP biology have been reported and summarized elsewhere [8, 9]. Herein we studied the impact of various MnPs on their ability to catalyze ascorbate oxidation leading to H_2O_2 production **(Figure 1)**. Comprehensive aqueous chemistry and cellular and mouse studies were conducted. In a subsequent study, we have addressed the Aim **(ii),** i.e. the ability of different redox-active drugs, including MnPs, to oxidize protein thiols in a GPx-like fashion [32].

EXPERIMENTAL

Chemicals

Porphyrin ligands, H_2T-2-PyP, H_2T-3-PyP and H_2T-4-PyP, were purchased from Frontier Scientific. Reagents needed for synthesis and purification of MnPs were purchased from the

sources detailed in [42, 50]. Plastic-backed silica gel TLC plates (Z122777-25EA) and (+)-sodium L-ascorbate (>98 %) were from Sigma-Aldrich. Acetonitrile (CH_3CN) and KNO_3 were purchased from Mallinckrodt. All chemicals were used as received without prior purification. All chemicals used to measure cellular thiol/disulfide redox states including reduced and oxidized glutathione, cysteine, cysteine, dansylchloride, iodoacetic acid, acetic acid, perchloric acid and methanol were purchased from Sigma-Aldrich.

Synthesis of Mn porphyrins

MnPs were synthesized and purified according to the procedures described elsewhere [42, 50-52].

Catalysis of ascorbate oxidation by MnPs

1) Spectrophotometric measurements of the initial rates of MnP-catalyzed ascorbate oxidation, $v_o(Asc)_{ox}$. Under our experimental conditions (pH 7.8), monodeprotonated form of ascorbic acid, HA^- (Asc) is a major species in aqueous solution of sodium ascorbate. In the reaction with $Mn^{III}P$ ascorbate is oxidized one-electronically to ascorbyl radical, $HA^\bullet$ which is readily deprotonated to $A^\bullet$. For details on ascorbic acid speciation see [8, 9, 33]. The $v_o(Asc)_{ox}$ were determined with 5 μM MnP and 0.15 mM sodium ascorbate under aerobic conditions at (25 ± 1)°C and at pH 7.8 (maintained with either 0.05 M Tris or potassium phosphate buffer). The buffer was initially treated with Chelex-100 ion-exchange resin (200-400 mesh sodium form, Bio-Rad Life Science) to remove adventitious transition metals present in solution. Ascorbate oxidation was followed at 265 nm on Shimadzu UV-2550 uv/vis spectrophotometer. The molar absorptivity of ascorbate was reevaluated to be ε_{265} = 14,000 M^{-1} cm^{-1}. The initial rates, $v_0(Asc)_{ox}$, (nMs^{-1}), were calculated based on the linear kinetic traces obtained for the first 60 seconds. The background rate for non-catalyzed ascorbate oxidation was subtracted from the rates for catalyzed reaction [33]. 2) Electrochemical measurements of initial rates of oxygen consumption, $v_0(O_2)_{red}$. Oxygen was consumed *via* reduction, thus initial oxygen consumption rates were described throughout text as $v_0(O_2)_{red}$. The experiments were carried out with Clark electrode at $(25\pm1)^0$C in either 0.05 M Tris or phosphate buffer, pH 7.8. Before measurement, the solutions were purged with air (~21% oxygen). The O_2^- sensitive Clark electrode (0.1 M KCl as filling solution) connected to a potentiostat was used. Potential of −0.8 V *vs* Ag/AgCl was applied to the electrode and once the initial current was stabilized (I_{max}, corresponding to the $[O_2]$ = 0.255 mM [53] in air-saturated solution) ascorbate solution was added at 1 mM concentration, followed by the addition of 10 μM MnP. The decrease in current, I_{obs}, corresponding to the decrease in O_2 concentration, $\Delta[O_2]$, was followed for at least 300 s. The solution was then purged with N_2 until the current was again stabilized (I_{min}, corresponding to the $[O_2] \approx 0$ mM). This allows for the calculation of O_2 concentration in the solution (in nM) as $[O_2]_{obs} = [(I_{obs} - I_{min}) \times 2.55\times10^5] / (I_{max} - I_{min})$, where I_{obs} is the current at any given time point. The initial reaction rate, $v_0 = -\Delta [O_2]_{obs} / \Delta t = -[(I_{obs2} - I_{obs1}) \times 2.55\times10^5] / [(I_{max} - I_{min}) \times (t_{obs2} - t_{obs1})]$, where I_{obs2} and I_{obs1} are currents at t_{obs2} and t_{obs1} time points related to a linear 60 s interval after the addition of MnP. The initial rates of ascorbate oxidation and oxygen consumption rates are given in nM s^{-1} **(Table 1** and **Figures 3** and **4)**.

Stability of MnPs towards oxidative degradation with H_2O_2 produced during MnP/ascorbate cycling

Stability of several MnPs (5 μM) used in cellular studies was determined in the presence of ascorbate (1 mM), and at pH 7.8 maintained by Tris buffer on UV-2550 PC Shimadzu spectrophotometer. The stability of other MnPs has been previously reported and discussed [42, 54, 55].

Lipophilicity determination

The TLC chromatographic retention factor, R_f (compound path/solvent path ratio) was determined for MnPs on silica gel plastic plates using 1:1:8=KNO_3(sat) H_2O:H_2O:CH_3CN as a solvent as earlier reported [55].

MRI studies

Measurements of T1 relaxivities were performed on 7.0 Tesla on a Bruker Biospec horizontal bore scanner with 0.1 mM MnP and 5 mM ascorbate in 0.05 M potassium phosphate buffer at (25±1)^{0}C [56]. T1-weighted images were processed using Paravision 4.0 software. The T1 relaxivities were calculated and expressed in mM^{-1} s^{-1}.

In vitro studies

Cell lines—Different mouse and human cell lines were used to explore the cytotoxicity of MnP/ascorbate system. 4T1 mouse mammary breast cancer cell line was purchased from Duke Cell Culture Facility. Human breast cancer cell lines MCF-7 and MDA-MB-231 as well as non-cancerous human breast epithelial cell line HBL100 were generous gift from Professor Christopher Ford and Professor Yunus Luqmani, Kuwait University. Monolayer cultures were grown at 37°C and 5% CO_2 in RPMI 1640 medium supplemented with 10% fetal bovine serum, 1% L-glutamine, 1% penicillin/streptomycin as an antibacterial agent and 0.1% amphotericin as an antifungal agent. For this experiment cultures were used at 70 – 90% confluency. Cell counting was performed with an improved Neubauer hemocytometer and trypan blue to differentiate between the viable and non-viable cells.

Cytotoxicity assay—Cytotoxicity of MnP/Asc system was assessed with 3-(4,5-dimethylthiazol-2-yl)-2,5-diphenyl-tetrazolium bromide (MTT) assay as previously described [57]. Cells were seeded into a flat-bottom 96-well microplate at a concentration of 5×10^4 cells/well and incubated overnight to adhere. Tested compounds were added at indicated concentrations in quadruplicate wells. Cells were incubated for 24 hours with either MnP or ascorbate or MnP/Asc. Control wells without MnP and ascorbate were incubated under same conditions. After incubation, the wells were washed with PBS, fresh medium was added followed by the addition of MTT reagent (10 μL per well). MTT reagent was prepared by dissolving 5 mg MTT in 1 mL PBS. Cultures were incubated for three hours at 37°C and then 10% SDS in 0.01 M HCl was added followed by overnight incubation. Absorbance was measured at 560 nm (formazan product) and 650 nm (background) using a microplate reader (Tecan Sunrise, Tecan Instruments). Results are presented as mean ± S.E. Differences were considered significant when $p < 0.05$ was achieved.

Cell proliferation assay—Effect of MnTE-2-PyP^{5+}/Asc on cell proliferation was investigated using the sulforhodamine B (SRB) assay on mouse breast cancer 4T1 and human breast cancer MDA-MB-231 cells. In brief, 15,000 cells/well were plated in quadruplicates onto a 96-well plate and left overnight to adhere. Five μM MnP was added concurrently with 1 mM ascorbate onto plate, and plates were kept in CO_2 incubator. Cell number was determined at 0, 24, 48, and 72 hours after the addition of MnP/Asc. Cells were fixed with ice cold trichloroacetic acid (TCA) at a final concentration of 10% and plates were kept in a refrigerator for an hour. Wells were then washed 5 times with deionized water. Fixed cells were stained with 0.4% sulforhodamine B dissolved in 1% acetic acid and dark-incubated for 25-30 minutes. Plates were carefully washed 5 times with 1% acetic acid to remove the excess dye and left to air dry. Bound dye was solubilized with 100 μL of 10 mM Tris. Absorbance was measured at 690 nm for the background and 510 nm for the dye.

Accumulation of MnPs in 4T1 cells in the presence and absence of ascorbate —To determine the MnP uptake, cells were seeded at a density of 3×10^5 cells per well in a 6-well plate. Cells were left for 24 h in CO_2 incubator to adhere. Then 5 μM MnP alone or in combination with 1 mM ascorbate were added. Catalase was added to each well in the amount of 1,000 U/mL to avoid cell damage by MnP/Asc-generated H_2O_2. Controls containing MnP plus catalase, and ascorbate alone, were tested in parallel. After incubation in CO_2 incubator, the wells were washed with PBS. The 1 mL of 2% SDS was then added to each well to solubilize the cells. After 24 h the content of each well was centrifuged for 10 minutes at 75,000 × g. The clear supernatant was used to measure the MnP content as previously described [58]. In brief, spectra were recorded and the area under Soret band quantified. Standard curve was used to assess the concentration of MnP in each sample. Standard curve was constructed by adding known concentration of MnP to solubilized, untreated cells. Separate standard curves were prepared for each compound. Protein levels were measured by Lowry method [59].

Measurements of redox states of GSH/GSSG and Cys/CySS in 4T1 cells—The 4T1 cells were seeded in 6-well plates at the density of 0.5×10^5 cells/well and allowed to reach ~80% confluence. They were then treated for 4 hours in a growth medium with MnTE-2-PyP^{5+} (5 μM or 15 μM) or ascorbate (1 mM or 3 mM) alone or in combination. Cells were washed 3 times with ice-cold PBS. Then 0.5 mL of the solution - consisting of 5% perchloric acid, 0.2 M boric acid and 10 μM γ-glutamylglutamate, γ-EE - was added, cells were scraped and transferred to microfuge tubes and centrifuged at 13,500 rpm for 1 min. The supernatants were transferred into new tubes for further derivatization as described elsewhere [60]. Concentrations of thiols and disulfides were determined by integration relative to internal γ-EE standard [61]. Reduction potential (*E*h) was calculated using GSH and GSSG, or Cys and CySS concentrations by Nernst equation as described previously [62]. Protein levels were determined by Thermo Scientific Pierce BCA Protein Assay Kit (cat# 23225).

Measurements of intracellular total thiol content—The 4T1 cells were treated as described above for GSH/GSSG and Cys/CySS measurements. They were harvested and

lysed by ultrasonication on ice. The intracellular thiol (RSH) content was determined as described in [63].

In vivo study

Mouse 4T1 breast cancer model—A total of hundred fifty-two 6-8 week-old female Balb/c mice weighing on average 20 g (Jackson Laboratory) were used. Two experiments were performed where either the impact of the dose of MnP (0.2 or 2 mg/kg/day), or the stage in the development of tumor (volume at the moment the treatments were initiated), on the tumor growth suppression were explored. In both studies, tumors were established *via* subcutaneous (sc) injection of 100 μL suspension of 10^6 cells into the mouse flank. In a 1st experiment, eighty mice were randomized into four treatment groups: **(1)** PBS (200 μL, intraperitoneally, ip); **(2)** Asc (4 g/kg/day, ip); **(3)** MnTE-2-PyP^{5+} (0.2 mg/kg/day, sc); and **(4)** MnTE-2-PyP^{5+} (0.2 mg/kg/day, sc) + Asc (4 g/kg/day, ip). Treatment started 24 hours post injection of tumor cell suspensions. In a 2nd experiment, once the tumor reached volume of ~80 mm^3, seventy-two mice were randomized into six groups: **(1)** PBS (200 μL, ip); **(2)** Asc (4 g/kg/day, ip); **(3)** MnTE-2-PyP^{5+} (0.2 mg/kg/day, sc); **(4)** MnTE-2-PyP^{5+} (2 mg/kg/day, sc); **(5)** MnTE-2-PyP^{5+} (0.2 mg/kg/day, sc) + Asc (4 g/kg/day, ip); and **(6)** MnTE-2-PyP^{5+} (2 mg/kg/day, sc) + Asc (4 g/kg/day, ip). Tumor volumes were measured daily with vernier digital caliper and calculated with formula: V = length × width × width × 1/2. The doses of MnP and ascorbate were based on those previously reported [45, 64]. Mice were treated for the duration of the study (15 days and 18 days for the 1st and 2nd experiment, respectively). The humane end point was set at an average tumor volume of 1,500 mm^3. To allow for the significant clearance of MnP from plasma [65], mice were sacrificed at 24 h post last treatment and tumors and muscles from the opposite leg excised and snap frozen in liquid nitrogen. No significant differences in mouse weights were found among treatment groups during the course of both experiments. Animal handlings and procedures were approved by Duke University Institutional Animal Care and Use Committee.

Statistical analysis—It was performed using a mixed-effects repeated measures model and a mixed-effects parametric survival-time model. First, the mixed-effects repeated measures model for ln(tumor volume) was estimated, including linear and quadratic time-trends, as well as interactions of time-trends with three treatment groups (Asc, MnP, and MnP/Asc, with baseline being the control group). A test conducted to evaluate the incremental effect of adding quadratic factors to the model was statistically significant (p-value is 0.0000). This test confirms a nonlinear relationship between time and ln(tumor volume) in the control and treatment groups. The model assumes mouse-specific random effects and an autoregressive correlation structure, of order one, within a mouse. In particular, it includes two mouse-specific random effects: random intercept and a random slope on the time variable at a mouse level (the model thus assumes that the effect of time could be mouse-specific). This model is estimated using the maximum-likelihood method. Additionally, pairwise comparisons between treatment groups were conducted (p-values were adjusted using Sidak correction in order to account for multiple comparisons). Second, the mixed-effects parametric survival-time model for the time the tumor volume reaches the endpoint at 1,500 mm^3 was applied. In particular, the random-effects Weibull model, with

normally distributed random effects within each mouse, was estimated using the maximum likelihood method with mode-curvature adaptive Gauss-Hermite quadrature integration method. All statistical analyses were carried out in STATA 14.0 Data Analysis and Statistical Software package.

Accumulation of MnTE-2-PyP^{5+} in tumor and muscle—The MnP levels in tumor and muscle were measured in the study where MnP was administered at 0.2 mg/kg/day. Tumors and muscles from opposite legs were homogenized and proteins removed from tissue with 1% acetic acid in methanol, solvent evaporated and residue reconstituted in LCMS/MS mobile phase. Analyses were performed on an Applied Biosystems MDS Sciex 4000 Q Trap LC/MS/MS spectrometer at Duke Cancer Institute, Pharmaceutical Research Shared Resource, PK/PD Core laboratory as detailed elsewhere [65].

RESULTS AND DISCUSSION

Over decades we have synthesized numerous Mn porphyrins [8, 9, 39, 66, 67]. We initially modified redox properties of Mn site (described by metal-centered reduction potential, $E_{1/2}$, for $Mn^{III}P/Mn^{II}P$ redox couple) to optimize MnPs as catalysts for $O_2^{\cdot -}$ dismutation [8, 9, 39, 66, 67]. It was subsequently shown that ability of MnPs to catalyze $O_2^{\cdot -}$ dismutation parallels their ability to reduce $ONOO^-$ [8, 9, 68]. It became soon obvious that bioavailability is another major factor that affects MnP therapeutic potential and can compensate for somewhat inferior redox properties [42, 54, 58]. Bioavailability is affected by the charge, size, shape, polarity and lipophilicity of MnPs. Our studies and studies of others demonstrate that, while SOD-like and $ONOO^-$ reduction activities are not excluded, some other processes may predominate *in vivo*. Such are those related to the coupling of MnPs with major cellular reductants, ascorbate and small molecular weight thiols (GSH, cysteine), as well as protein thiols [8, 9]. We have already indicated that cationic *ortho* Mn(III) *N*-substituted pyridyl-porphyrins bear therapeutic potential as catalysts for ascorbate oxidation with concomitant production of cytotoxic H_2O_2 [33, 45, 69]. H_2O_2 can subsequently be employed by MnP to oxidize or *S*-glutathionylate critical protein thiols, thereby affecting cell survival pathways [8-11, 32, 70] (**Figure 2**).

H_2O_2-mediated therapeutic effects of MnPs

Work done by Tome's group [10, 11] was instrumental in providing undoubted evidence that cytotoxicity of MnP/dexamethasone to lymphoma cell (but not to normal lymphocytes) is due to the production of high levels of H_2O_2. H_2O_2 was subsequently used by MnP/GSH to catalyze *S*-glutathionylation of p65 subunit of NF-κB. In turn, levels of H_2O_2 remained unchanged. When either H_2O_2 or GSH is removed no *S*-glutathionylation was observed [10].

Tome's group subsequently showed that other protein thiols have been modified also with subsequent loss of protein activity. Complexes I, III and IV of mitochondrial respiration were *S*-glutathionylated with MnP/H_2O_2/GSH which led to the inhibition of complexes I and III and suppression of ATP production. When MnP was coupled with 2-deoxyglucose, the glycolysis was suppressed accompanied with suppression of ATP [10]. *S*-glutathionylation of glycolysis proteins likely plays role also. In turn MnP/H_2O_2 suppressed

both mitochondrial and glycolytic energy sources of cancer cell, while not being harmful to normal lymphocytes [10]. Both cytosolic and mitochondrial actions of MnP/H_2O_2 play role in MnP therapeutic effects. While *S*-glutathionylation of p65 subunit of NF-κB and glycolysis, as well as phosphorylation of ERK [33] happen in cytosol ([11] and refs therein), the impact of MnP on electron transport chain is a clear mitochondrial event. Nucleus may be involved also in the actions of MnPs: Piganelli's group suggested (based on an indirect evidence) that MnTE-2-PyP^{5+} oxidizes p50 subunit of NF-κB at the level of nucleus preventing in turn the DNA binding of NF-κB - such suggestion was supported by 3-fold higher levels of MnP in nucleus than in cytosol [21, 36]. Several studies by St. Clair's group showed the effect of MnPs at mitochondrial level also [71-73].

Once the key impact of H_2O_2 in the actions of MnP was identified, we started understanding the mechanism of MnP radio- and chemosensitizing effects [2, 8], We also realized the therapeutic potential of MnP/Asc system as a source of H_2O_2 in its own right, but also when combined with additional sources of H_2O_2 - radiation or chemotherapy. Radio- and chemotherapy have always been standard of care with patients who are recruited for prospective Clinical Trials. We undertook this study to identify those properties of MnP that affect its ability to cycle with ascorbate thereby producing H_2O_2 and to correlate such ability with cytotoxicity to cells and tumors. Studies are also in progress to understand the impact of the chemical and physical properties of MnP on a subsequent step - MnP/H_2O_2/GSH-driven oxidation of protein thiols [32, 74].

Cancer-related pathways, affected specifically by the MnP/Asc H_2O_2-producing system, were studied on inflammatory breast cancer cell SUM149. The data correlate well with lymphoma studies [10, 11]. The study indicated that both cytosolic and mitochondrial pathways are involved, and that at least in part NF-κB was a key player involved in MnP/Asc toxicity [33]. GSH was found to play major role also, and catalase eliminated the toxicity. MnP/Asc system was able to reduce GSH levels and phosphorylate NF-κB and ERK (extracellular signal-regulated kinase). The X-linked inhibitor of apoptosis protein, XIAP, was decreased and annexin V increased indicating apoptosis-related cytotoxicity imposed by MnP/Asc system. In addition, the translocation of apoptosisinducible factor, AIF, into nucleus implicates AIF-mediated and caspase-independent SUM 149 cell death pathway.

The interaction of ascorbate with other redox-active compound, menadione, has been explored and clinically tested. An oral combination of ascorbate and menadione (Apatone) has been evaluated as an anticancer agent in a clinical study in prostate cancer patients who had failed standard therapy. Promising delay in the biochemical progression of the disease was observed in Apatone-treated patients. Indeed, a significant increase in the PSA (Prostate Serum Antigen) doubling time was induced by Apatone treatment without dose-limiting adverse effects [75-77].

Fourteen MnPs (**Figure 1**) were evaluated in this work with the goal to: **(1)** identify the best catalyst(s) of ascorbate oxidation among existing Mn porphyrins and to correlate such data with their thermodynamic and kinetic properties most so with their SOD-like potency; **(2)** show that the magnitude of the catalysis of ascorbate oxidation parallels the magnitude of

the cellular cytotoxicity of MnP/Asc system; and **(3)** evaluate the tumor cytoxicity of best catalyst in a mouse model. These MnPs studied differ largely with respect to $E_{1/2}$, charge, size, shape, bulkiness, polarity and lipophilicity. Among these compounds, $MnTBAP^{3-}$ is anionic and disfavors reaction with negatively charged ascorbate on both thermodynamic and electrostatic grounds. All other porphyrins are positively charged. Among them there are MnPs with short and long linear pyridyl substituents. Some bear polar oxygen atoms embedded within linear substituents. Two MnPs have cyclic substituents and are therefore very bulky. Few MnPs are hydrophilic, but many are lipophilic. Among lipophilic MnPs, some are polar due to the presence of oxygens within pyridyl side-chain substituents. We have described the ability of MnPs to catalyze ascorbate oxidation with initial rates of ascorbate oxidation ($v_0(Asc)_{ox}$), and initial rates of oxygen consumption/reduction ($v_0(O_2)_{red}$). We have discussed kinetic data with respect to the thermodynamic properties of Mn site ($E_{1/2}$ of $Mn^{III}P/Mn^{II}P$). We then explored the ability of seven most characteristic MnPs to induce cytotoxicity to three breast cancer (human MCF-7 and MDA-MB-231 and mouse 4T1) and non-cancerous epithelial breast cell (human HBL100). We finally conducted *in vivo* study on the suppression of 4T1 tumor growth in a mouse sc flank model.

Aqueous chemistry of MnP/Asc system - Reduction potential of MnP controls Asc oxidation rate

The ability of MnPs to catalyze ascorbate oxidation was assessed by direct (spectrophotometrical) and indirect (electrochemical) means (**Figure 2**) *via* measuring initial rates of ascorbate oxidation ($v_0(Asc)_{ox}$, **Table 1** and **Figure 3**) and initial rates of oxygen reduction, ($v_0(O_2)_{red}$, **Table 1** and **Figure 4**). The metal-centered reduction potential, $E_{1/2}$, as a measure of MnP redox properties and R_f, as a measure of their lipophilicity are also listed in **Table 1**.

Initial rates, $v_0(Asc)_{ox}$ and ($v_0(O_2)_{red}$, are related to $E_{1/2}$ in a bell shape fashion (**Figure 3B** and **4B**). MnPs with negative $E_{1/2}$ (such as $MnTBAP^{3-}$ and $MnTE\text{-}2\text{-}PyPhP^{5+}$) have very low initial rates. Such compounds cannot be easily reduced with ascorbate in a 1st step of catalytic cycle (**Figure 2**). In addition, anionic $MnTBAP^{3-}$ would have been repelled from negatively charged monodeprotonated ascorbate [8, 9]. Conversely, those MnPs with too positive potential are readily reduced to the Mn +2 oxidation state but are difficult to be oxidized back to the Mn +3 state to close the catalytic cycle (**Figures 2, 3,** and **4**). Under aerobic conditions, due to high oxygen levels, the reoxidation of MnP will likely occur with O_2 [33]. The steric hindrance towards the approach of ascorbate to Mn site of bulky molecules, such as $MnTPhE\text{-}2\text{-}PyP^{5+}$ (**Figs. 3C and 4B**), $MnTnHexOE\text{-}2\text{-}PyP^{5+}$, and $MnTnOct\text{-}2\text{-}PyP^{5+}$, contributes also to the lower values of $v_0(Asc)_{ox}$ relative to $MnTE\text{-}2\text{-}PyP^{5+}$.

Such impact of $E_{1/2}$ on ascorbate oxidation coincides with the optimal $E_{1/2}$ for the catalysis of $O_2^{\cdot -}$ dismutation; the reasoning being similar. Like SOD enzyme, its mimic must be able to equally efficiently oxidize and reduce $O_2^{\cdot -}$, thus operating at $E_{1/2}$ which is right in between the reduction and oxidation potential of $O_2^{\cdot -}{}_2$, in the range of ~ +200 to ~ +400 mV *vs* NHE [42]. It is important to note that SOD-like ability of MnPs parallels their ability to undergo all reactions thus far studied, such as reduction of $ONOO^-$ [68], catalase-like

activity [54], ability to catalyze ascorbate oxidation (this work) and ability to mimic GPx enzyme [32].

The ascorbate oxidation was followed in Tris and phosphate buffers at pH 7.8. Those buffers differ with regards to hydrogen bonding. The difference between the Mn/ascorbate kinetics in those two buffers was prominent with those MnPs which have the largest affinity for hydrogen bonding: MnTnBuOE-2-PyP^{5+} and MnTnHexOE-2-PyP^{5+} (**Figures 3** and **4**). The hydrogen of the protonated Tris buffer could form hydrogen bonding with the oxygen atom of the oxygenated butoxyethyl or hexoxyethyl side chains of MnTnBuOE-2-PyP^{5+} and MnTnHexOE-2-PyP^{5+}. This would increase the net positive charge of MnP, which in turn could enhance the guidance of the negatively charged ascorbate towards Mn site. The strong impact of Tris relative to phosphate buffer on the kinetics of ascorbate oxidation by alkoxyalkyl derivatives suggests that it is still difficult to fully predict the magnitude of the therapeutic effects of MnPs in a very complex milieu of a cell. This is particularly true in the case of those MnPs that bear different amphiphilic features which allow diverse interactions with various biomolecules: 5 positive charges, alkyl chains, oxygen atoms, cationic electron-deficient Mn site favoring axial ligation of different species.

Lipophilicity of MnPs

The lipophilicity of MnPs, described with chromatographic retention factor R_f, along with their $E_{1/2}$ values are plotted in **Figure 5**. We have explored MnPs of diverse properties: those that are hydrophilic (such as MnTE-2-PyP^{5+}) and lipophilic (MnTnOct-2-PyP^{5+}) but have favorable $E_{1/2}$ that allows them to cycle with ascorbate. We have also studied those that are lipophilic but whose $E_{1/2}$ limits their cycling with ascorbate (such as MnTE-2-PyPhP^{5+}). Among lipophilic compounds MnTnHexOE-2-PyP^{5+} is polar as it bears oxygen atoms in pyridyl substituents, while MnTnOct-2-PyP^{5+} bears apolar long alkyl chains. Polar oxygen atoms largely influence the reactivity of MnTnHexOE-2-PyP^{5+} towards ascorbate (see discussion in *Aqueous Chemistry of MnPs*). Some lipophilic compounds bear linear substituents such as MnTnOct-2-PyP^{5+}, while a lipophilic MnTPhE-2-PyP^{5+} has aromatic rings as *N*-substituents. These rings affect the lipophilicity of MnTPhE-2-PyP^{5+} and make it bulkier, and in turn restrict its accumulation within cell (see discussion under Accumulation MnPs in 4T1 cells in the absence and presence of ascorbate. The interplay of those properties affect reaction of MnPs with ascorbate and their accumulation within cell where MnP/H_2O_2 driven oxidation of signaling proteins, affecting cell survival, takes place.

Magnetic resonance imaging studies

Mn porphyrins—Mouse prostate cancer study indicated that MnTE-2-PyP^{5+} and MnTnHex-2-PyP^{5+} have potential as MR imaging agents being superior to commercially available gadolinium chelates [56]. We have therefore explored different MnPs on their MRI properties in the presence and absence of ascorbate, our major endogenous antioxidative defense. The difference in the relaxivities of paramagnetic MnPs stems mainly from the difference in the degree of interaction of the paramagnetic Mn with water protons in the inner coordination sphere of its porphyrin complex [78-80]. In Mn^{III}P, the Mn +3 has 4 unpaired *d* electrons and two water molecules in axial positions that are available for exchange with bulk waters. Our MRI aqueous studies demonstrated that T1 relaxivity

depends upon MnP ability to exchange axial water with bulk waters. T1 relaxivity is thus controlled by the strength of axial Mn-H_2O bond, which is best described by the deprotonation constant for 1st axial water, p$K_{a(ax)}$. Steric factors were also found to play a role, giving rise to a bell-shaped relationship between the T1 relaxivity and p$K_{a(ax)}$ (**Figure 6**). We have reported that p$K_{a(ax)}$ is linearly but inversely correlated with $E_{1/2}$ [54, 81]. When the p$K_{a(ax)}$ decreases (from ~ 12 to ~11), as anticipated, the $E_{1/2}$ increases. The drop in p$K_{a(ax)}$ (increase in $E_{1/2}$) from $MnTBAP^{3-}$ and MnTE-2-$PyPhP^{5+}$(#1) to MnTE-3-PyP^{5+}(#2) and to MnTE-2-PyP^{5+}(#3) is accompanied by strengthening of Mn-H_2O bond, which lowers the water-exchange rates and causes the T1 relaxivity to drop (**Figure 6B** and **6C**). Yet T1 relaxivity increases as MnPs [MnTPhE-2-PyP^{5+}(#4), MnTnHexOE-2-PyP^{5+}(#5) and MnTnOct-2-PyP^{5+} (#6)] become bulky (regardless of further drop in their p$K_{a(ax)}$ values), giving rise to a bell shape relationship (**Figure 6B** and **6C**).

Our MRI results are in agreement with data published on the water exchange rates of several MnPs [82]. Anionic $MnTSPP^{3-}$ ($E_{1/2}$ = −160 mV *vs* NHE) and $MnTBAP^{3-}$ ($E_{1/2}$ = −194 mV *vs* NHE) have similar redox properties, overall charge and stericity. $MnTSPP^{3-}$ has p$K_{a(ax)}$ of 12.3, while the p$K_{a(ax)}$ of $MnTBAP^{3-}$ is 12.6. Thus, relative to MnTE-2-PyP^{5+} (p$K_{a(ax)}$ =10.7), with less stronger binding of axial water, $MnTSPP^{3-}$ has >10-fold higher $k_{ex}(H_2O)$. While of similar pK_{a1} values (10.7 vs 11), larger stericity of MnTnHex-2-PyP^{5+} relative to MnTE-2-PyP^{5+} resulted in ~40% larger $k_{ex}(H_2O)$. Most likely the same steric factors valid for MnTnHex-2-PyP^{5+} contribute to the increase in T1 relaxivity of even bulkier molecules, MnTPhE-2-PyP^{5+}(#4), MnTnHexOE-2-PyP^{5+}(#5) and MnTnOct-2-PyP^{5+}(#6), relative to MnTE-2-PyP^{5+} despite similar p$K_{a(ax)}$ values [54].

Mn porphyrins + ascorbate—Ascorbate affects T1 relaxivity of only those MnPs which are easily reducible (**Figure 6A** and **B**). The T1 relaxivity drops as $Mn^{III}P$ gets reduced. It has been argued that the elongation of the effective electron spin density of the manganese center in the direction of the bound water molecules is mostly responsible for the large increase in the relaxivity of $Mn^{III}P$ (with Mn in +3 oxidation state) when compared to other potential contrast agents such as Gd^{3+} [$Gd(DTPA)^{2-}$] and Mn^{2+} chelates [$Mn(EDTA)^{2-}$] [56, 83, 84]. The point dipole approximation that predicts a spherical distribution of the electron cloud of manganese in S-state ions such as Gd^{3+} and Mn^{2+}, does not hold for $Mn^{III}P$, since the electron spin density of Mn +3 in $Mn^{III}P$ complex is closer to the protons of the bound waters [83-85]. The increased dipolar interaction results in a shorter distance (r) between the metal center and the water protons. The paramagnetic effect is inversely proportional to r, resulting in higher relaxivity of $Mn^{III}P$ than for Mn^{2+} with S-state electron configurations.

Stability of MnPs towards Asc-mediated oxidative degradation

Stabilities of several MnPs explored in cellular studies are shown in **Figure 7**. The most stable compounds are those ($MnTBAP^{3-}$ and MnTE-2-$PyPhP^{5+}$) which are either not at all, or only slightly reducible with ascorbate (exemplified with negative values of $E_{1/2}$). Due to the lack ($MnTBAP^{3-}$) or very slow (MnTE-2-$PyPhP^{5+}$) rate of ascorbate oxidation either no or very small amount of H_2O_2 is produced in the medium. This results in their negligible degradation (**Figure 7**, shown for MnTE-2-$PyPhP^{5+}$). MnTE-2-PyP^{5+} demonstrates higher

stability than its *meta(3)* analog, MnTE-3-PyP^{5+}. Our data suggest that oxidative degradation proceeds *via* Mn +3 oxidation state. In turn *meta(3)* analog, MnTE-3-PyP^{5+} which rapidly re-oxidizes to Mn +3 oxidation state is the least stable among MnPs studied (**Figure 7**). The *ortho(2)* MnPs (MnTE-2-PyP^{5+}, and MnTPhE-2-PyP^{5+}) with ~200 mV higher $E_{1/2}$ than MnTE-3-PyP^{5+} are stabilized in Mn +2 oxidation state, resist re-oxidation and in turn oxidative degradation (**Figure 7).** The data agree well with reported data on H_2O_2-driven oxidative degradation of methyl isomers, MnTM-2(or 3 or 4)-PyP^{5+} [82]. The $E_{1/2}$ of MnTnHexOE-2-PyP^{5+} and MnTnOct-2-PyP^{5+} is 139 or 85 mV higher than that of MnTE-2-PyP^{5+}. Therefore they are further stabilitized in Mn +2 state and are thus less prone to close the catalytic cycle. The consequence of such behavior is **(i)** lower ability to catalyze ascorbate oxidation and **(ii)** lower affinity towards degradation. Additionally both are bulky molecules which further reduces their catalytic potency (see **Table 1**, **Figure 3, Figure 4**, and *Cytotoxicity of MnP/Asc* data below).

In vitro studies

Cytotoxicity of MnP/Asc

MnP/Asc is cytotoxic to breast cancer cells: Seven MnPs, with $E_{1/2}$ ranging from −194 to +340 mV *vs* NHE (**Figure 3C** and **4C),** were selected to explore the impact of ascorbate oxidation rate on the cytotoxic potential of MnP/Asc system. The choice of compounds exemplifies diverse properties of MnPs catalytic potency in aqueous solutions.

Bell-shape relationship between $E_{1/2}$-controlled $v_o(Asc)_{ox}$ and MnP/Asc-mediated cellular cytotoxicity: Redox property of MnP, described by $E_{1/2}$, which controls the catalysis of ascorbate oxidation has also major impact on MnP/Asc-induced cellular cytotoxicity (**Figures 7-9**). Steric and electrostatic factors (see *Aqueous Chemistry of MnP/Asc*), as well as stability of MnPs towards H_2O_2-driven oxidative degradation (see below) play also a role (**Figure 7**). The highly negative $E_{1/2}$ of −194 mV *vs* NHE precludes reduction of MnTBAP^{3-} with ascorbate (**Figures 3** and **4)**, and in turn deemed it nontoxic to cells (**Figures 8** and **9)**. With $E_{1/2}$ = −65 mV *vs* NHE, MnTE-2-PyPhP^{5+} has already modest ability to catalyze ascorbate oxidation. Thus it induced cell death at higher concentrations than those MnPs with higher $E_{1/2}$; its modest lipophilicity contributes favorably to its modest effect (**Figures 8 and 9**). Its catalytic potency is though much lower than that of two lipophilic MnPs of favorable $E_{1/2}$ values: MnTnHexOE-2-PyP^{5+} ($E_{1/2}$ = +313 mV *vs* NHE) and MnTPhE-2-PyP^{5+} ($E_{1/2}$ = +259 mV *vs* NHE). The bulkiness of MnTnOct-2-PyP^{5+} precludes an easy access of ascorbate to Mn site deeply buried within cavity encircled with long alkyl chains. In addition its high $E_{1/2}$ of +367 mV *vs* NHE stabilizes it in +2 oxidation state disfavoring thus closing a catalytic cycle. The lipophilic octyl side-chains contribute to MnTnOct-2-PyP^{5+} toxicity as a single agent (**Figure 10**). Though MnTnHexOE-2-PyP^{5+} is also bulky, the presence of oxygen atoms in its pyridyl side-chain substituents facilitate the approach of ascorbate. It also has 50 mV less positive $E_{1/2}$ and would thus favor re-oxidation more than does MnTnOct-2-PyP^{5+}. In turn, MnTnHexOE-2-PyP^{5+} is a better catalyst than MnTnOct-2-PyP^{5+} (**Figures 3 and 4**) and when combined with ascorbate it induces higher cellular cytotoxicity MnTnOct-2-PyP^{5+}/Asc (**Figure 8 and 10**). A very similar pattern demonstrated with 4T1 was seen with human breast cancer cell line MCF-7

and MDA-MB-231 (**Figure 10**). With all cell lines and among those MnPs studied, MnTE-2-PyP^{5+} bears the highest potential as an anticancer drug when combined with ascorbate. Importantly, MnPs alone exhibit either slight or no toxicity towards cancer cells. The toxicity of MnTnOct-2-PyP^{5+} is primarily due to its long lipophilic octyl chains.

Cytotoxicity is primarily due to the extracellular H_2O_2 production: Our earlier observations [8, 9, 44, 45], and studies of others [49, 86], as well as the impact that catalase has in preventing cytotoxicity of MnP/Asc (exemplified on MDA-MB-231 in **Figure 10**), demonstrated that cytotoxicity is primarily due to the MnP cycling with ascorbate outside of cell. The production of H_2O_2 within cell, though, cannot be fully excluded; the minor impact of lipophilicity has been observed. When cells (MCF-7) were pre-incubated with MnPs, and washed afterwards, slight sensitivity towards ascorbate was observed (data not shown).

The cytotoxicity is also dependent upon the stability of MnP catalyst towards oxidative degradation: Due to ~180 mV less positive $E_{1/2}$, which facilitates its re-oxidation (from $Mn^{II}P$ to $Mn^{III}P$), *meta* MnTE-3-PyP^{5+} is more prone to oxidative degradation with H_2O_2 than are *ortho* MnPs studied (**Figure 7**). Lower stability likely accounts for its lower cytotoxicity at higher concentrations, where MnTE-3-PyP^{5+} is rapidly degraded with H_2O_2 in the medium due to its generation and accumulation (**Figure 8).** The 10-fold higher lipophilicity of MnTE-3-PyP^{5+}, however, likely compensate for its lower stability relative to MnTE-2-PyP^{5+} resulting in similar cytotoxicities at lower concentrations (**Figures 8** and **9**). Once within cell, H_2O_2 is used by MnP in the catalysis of protein oxidation which ultimately results in suppression of tumor growth [8, 9]. Thus the lipophilicity of MnPs, affecting their cellular uptake, plays also a role.

In summary, the interplay between the redox property, lipophilicity, and stericity/bulkiness of MnPs, which affect MnP/Asc-induced H_2O_2 production, its utilization in oxidative damage of proteins and MnP cellular uptake, controls the magnitude of in vitro and in vivo anticancer effects.

Being identified as the best catalyst among MnPs studies, MnTE-2-PyP^{5+} was tested additionally in a cell proliferation assay. The data clearly show that MnP/Asc completely blocked cell proliferation (**Figure 12**).

MnP/Asc is not cytotoxic to non-cancerous breast cell line: The sensitivity of non-cancerous cell to MnP/Asc treatment was also studied. At the concentrations used, and under the conditions of this study, none of MnPs was toxic to non-cancerous human breast epithelial cell line HBL-100 in the presence of ascorbate (**Figure 12**). Only MnTnOct-2-PyP^{5+} when applied alone inflicted toxicity due to its excessive lipophilicity and likely surfactant effect arising from its long lipophilic alkyl chains.

Our data on cell cytotoxicity agree well with the data published earlier on several other cancer and normal cell lines. Thus, MnP/Asc system was toxic to 3 different human glioma cell lines, but not to normal astrocytes [47]. It was also toxic to MCF-7 and HeLa cells, but not to normal human dermal fibroblasts, NHDF [8].

MnPs accumulation in 4T1 cells in the absence and presence of ascorbate— Based on our and data of others, under *in vitro* conditions, cytotoxic H_2O_2, produced in the medium (in the reaction of MnP with ascorbate) enters the cell where it exhibits cytotoxicity *via* reactions catalyzed by MnPs [33, 41, 54]. In turn accumulation of MnPs is anticipated to play a role in anticancer effects of MnPs. The study was therefore conducted to determine the accumulation of MnPs and the impact ascorbate has on it. Modest increase in MnP accumulation in 4T1 cells has been observed in the presence of ascorbate and was pronounced with those MnPs that could be reduced with ascorbate (**Figure 13**). Thus, no impact of ascorbate was observed on cellular uptake of $MnTBAP^{3-}$. The accumulation of $MnTE\text{-}2\text{-}PyP^{5+}$ in 4T1 cells agrees well with the data on its accumulation in tumors derived from 4T1 cells (**Figure 15B**) where no major effect of ascorbate was also seen. As anticipated, a more lipophilic MnPs, such as $MnTPhE\text{-}2\text{-}PyP^{5+}$, $MnTnHexOE\text{-}2\text{-}PyP^{5+}$ and $MnTnOct\text{-}2\text{-}PyP^{5+}$, accumulate in 4T1 cells to a larger extent than more hydrophilic MnPs, such as $MnTE\text{-}2\text{-}PyP^{5+}$ and $MnTE\text{-}3\text{-}PyP^{5+}$ (**Figure 13**).

MnP/Asc increases 4T1 cell oxidative burden—Earlier studies clearly indicated that MnP/Asc is a source of H_2O_2 which MnP employs for oxidative modifications of signaling proteins inducing in turn cytotoxicity [33, 45]. Herein we demonstrated that MnP/Asc system deprives cells from thiol-derived reducing equivalents. The MnP/Asc-driven oxidation of glutathione and cysteine in 4T1 cells allowed us to quantify the changes in cellular reduction potential towards more oxidative environment (**Figure 14**). Levels of reduced global thiols, RSH, (**Figure 14A)** and glutathione, GSH, (**Figure 14B)** were significantly lower in the cells treated with the MnP/Asc relative to those cells that received single treatments. Based on the ratios of oxidized and reduced glutathione (GSSG/GSH) and cysteine (CySS/Cys), the cellular reduction potentials were calculated and are shown in **Figure 14C** and **D**. Our results demonstrate that MnP/Asc imposes higher oxidative burden on cell redox environment than either treatment alone. Data agree well with the results on redox proteomics to be addressed in a subsequent publication.

In vivo study

Mouse flank tumor study

Tumor growth suppression by MnTE-2-PyP/Asc in a sc mouse flank model: Our data on $MnTnHex\text{-}2\text{-}PyP^{5+}$/Asc system in a 4T1 mouse flank tumor model suggested its anticancer potential [45]. Only trend towards significance was, though, demonstrated because **(i)** the treatment started when tumor was already in aggressive phase of growth (volumes averaging ~250 mm^3), and **(ii)** $MnTnHex\text{-}2\text{-}PyP^{5+}$ is not a very good catalyst of ascorbate oxidation (**Figures 3** and **4**). Also the toxicity, due to fairly high dosing of a very lipophilic MnP, might have outbalanced its efficacy [8, 9].

Among MnPs characterized, $MnTE\text{-}2\text{-}PyP^{5+}$ has the highest ability to catalyze ascorbate oxidation in aqueous system and the highest anticancer efficacy in cellular studies exemplified herein with 3 breast cancer cell lines (**Figures 8-10**). The proliferation assay demonstrated that $MnTE\text{-}2\text{-}PyP^{5+}$/Asc treatment inhibits cancer cell proliferation (**Figure 11**). It was therefore forwarded to a mouse flank 4T1 breast cancer model. Two studies were done. In a 1^{st} study either 2 or 0.2 mg/kg/day dose of MnP was tested in combination with

pharmacological dose (4g/kg/day) of ascorbate, and treatment started once tumors on average reached 80 mm^3. In a 2nd study MnP/Asc treatment started 24 h after the injections of tumor cells (**Figure 15A**). As similar tumor suppression was observed in either study, early start of treatment appears not to be necessary. Early in development tumor has neither developed its vasculature, nor are the supporting cells, such as macrophages, infiltrated into its mass. Those events likely play role in the actions of MnPs [6, 45, 87].

Statistical analysis, namely the estimated mixed-effects repeated measures model, demonstrated that MnP/Asc treatment has significant tumor growth suppression compared to PBS-treatment group ($p<0.01$). As tumor continued growing, the impact of MnP/Asc became more pronounced (**Figure 15A**). In particular, for days 12-15, pairwise comparisons show that differences between MnP/Asc group vs each of PBS, Asc and MnP groups were statistically significant, $p<0.05$. On day 15th, the majority of mice in PBS, Asc and MnP treatment groups (>60%) had a tumor volume larger than 1,500 mm^3, while in the MnP/Asc treatment group 95% of animals remained under this threshold (namely, 19 out of 20 mice), as shown in **Figure 15B**. Furthermore, the results of the survival-time model estimation suggest that the MnP/Asc treatment has a statistically significant negative effect on the tumor reaching 1,500 mm^3 volume, compared to PBS-treatment group ($p=0.0008$). The differences between the effects of the MnP/Asc treatment and that of Asc and MnP treatments are also statistically significant at a level lower than 1% (p-values are 0.0010 and 0.0017, respectively). These results thus suggest that mice under the MnP/Asc treatment have a significantly higher probability of not reaching the tumor volume of 1,500 mm^3 than other three groups (PBS, Asc, and MnP) within the time-period studied.

Several different MnPs have recently been explored on their *in vivo* anticancer potential in presence of combined sources of H_2O_2 - MnP/Asc and radiation [46]. The addition of radiation profoundly amplified the anticancer effect of MnP/Asc [46].

Some of the cancer-related pathways associated with treatment, where Mn was coupled with RT-driven H_2O_2 production, have been assessed. The gene profiling of human D 245-MG glioma growing on Balb/c nu/nu mouse flank showed that MnTnBuOE-2-PyP^{5+}/RT, relative to RT, down-regulated metastatic pathways (*ctss*, catepsin L, *becn1*, beclin1) as well as anti-apoptotic and NF-κB pathways (*Nfkb1*, *Bcl211*, *Bcl2*) and PI3kinase and mTOR (*Rsp6kb1*). The protein translation changes were implicated also (*EIF5b* and *Rsp6kb1*) [8]. The collaborative efforts of ours and Dean Jones's group on MnP/Asc-driven impact on redox proteomics support such observations [manuscript in preparation].

Preferential accumulation of MnP in tumor relative to normal tissue—Ascorbate does not significantly affect accumulation of MnTE-2-PyP^{5+} in either tumor or muscle. However large difference in MnP accumulation (of ~7-fold) was found in tumor *vs* normal tissue (**Figure 15B**). Such selectivity in MnP accumulation, along with high ascorbate accumulation in tumor *via* Glut transporters [88], substantiates differential impact of MnP, in the presence of exogenous source(s) of H_2O_2, on tumor *vs* normal tissue.

Concluding remarks

It has been well documented that, when compared to normal tissue, tumor is frequently under oxidative stress, *i. e.* has high levels of H_2O_2 [8, 9, 15-31]. The magnitude of oxidative stress depends upon the stage of tumor development and is frequently due to the lower expression and/or activity of endogenous antioxidative defenses as well as to the perturbed ratio of superoxide dismutases (most so MnSOD) to enzymes that controls the H_2O_2 levels, such as catalases, GPx and peroxiredoxins [8, 9, 15, 17-31]. Similar to MnP/radiation and/or MnP/chemotherapy, MnP/Asc system was explored as an anticancer strategy to increase tumor H_2O_2 levels [2, 6, 8-11, 33, 45-47, 64]. Cycling of MnP with ascorbate primarily happens in extracellular space [33, 40, 41, 64]. Once produced, H_2O_2 enters cancer cell. There it gets utilized by MnP in the catalysis of H_2O_2-driven protein thiol oxidation or *S*-glutathionylation in a GPx-like fashion [8-11, 21, 23, 36, 67, 89]. In turn, pro-apoptotic pathways might be activated. Along with high tumor H_2O_2 levels and high ability of MnP to catalyze ascorbate oxidation, ~7-fold higher accumulation of MnP in tumor *vs* normal tissue as well as preferential tumor accumulation of ascorbate [88, 90-92], dictate differential impact of MnP/Asc treatment seen elsewhere: suppression of tumor growth, while healing of normal tissue injury inflicted during cancer chemo- or radiotherapy [1, 2, 8]. The differential effects upon tumor and normal tissue agree well with the data from cellular studies where cytotoxicity was seen with different cancer but not normal cells (this work and [8, 47]). In the presence of exogenous H_2O_2, tumor protection by MnP has never been observed [1, 2, 8, 9, 33, 45-47]. Our data on H_2O_2-related chemistry and biology of MnPs (this work and [54, 74]) contribute to the understanding of differential effects of MnPs [1-4, 6-11, 33, 45-47, 64, 93-95].

The ability of MnP to amplify anticancer effect, in the environment where H_2O_2 is produced, carries large therapeutic potential. The production of H_2O_2 *via* cycling of MnP with ascorbate, and in turn the resulting anticancer effect could be further enhanced with additional source(s) of peroxide such as chemotherapy [48, 93, 94] and radiation [8, 46, 95].

ACKNOWLEDGEMENT

IBH, AT and IS acknowledge NIH 1R03-NS082704-01, NIH U19AI067798, and BioMimetix JVLLC (USA). AT acknowledges mini-fellowship award from SFRBM. IS is grateful for the support to 5-P30-CA14236-29. JSR, JCBJ and RSP acknowledge CNPq and CAPES from Brazil. LB, BHB and MT acknowledge support by grants MB02/12, YM04/14 and SRUL02/13 from Kuwait University. DJ and YG acknowledge NIH R01 ES023485 and R21 ES 025632. IBH and IS are consultants with BioMimetix JVLLC and hold equities in BioMimetix JVLLC. IBH, IS and Duke University have patent rights and have licensed technologies to BioMimetix JVLLC.

ABBREVIATIONS

$O_2^{\bullet-}$	superoxide
$ONOO^-$	peroxynitrite
γ-EE	γ-glutamylglutamate
$MnTBAP^{3-}$	Mn(III) *meso*-tetrakis(4-carboxylatophenyl)porphyrin

MnTE-2-PyP^{5+}	AEOL10113, BMX-010, Mn(III) *meso*-tetrakis(*N*-ethylpyridinium-2-yl)porphyrin
MnTE-3-PyP^{5+}	Mn(III) *meso*-tetrakis(*N*-ethylpyridinium-3-yl)porphyrin; MnTE-3-PyP^{5+}
MnTE-4-PyP^{5+}Mn(III)	*meso*-tetrakis(*N*-ethylpyridinium-4-yl)porphyrin
MnTnPen-4-PyP^{5+}	Mn(III) *meso*-tetrakis(*N*-npentylpyridinium-4-yl)porphyrin
MnTnHex-2-PyP^{5+}	Mn(III) *meso*-tetrakis(*N*-n-hexylpyridinium-2-yl)porphyrin
MnTnHex-3-PyP^{5+}	Mn(III) *meso*-tetrakis(*N*-n-hexylpyridinium-3-yl)porphyrin
MnTnHex-4-PyP^{5+}	Mn(III) *meso*tetrakis(*N*-n-hexylpyridinium-4-yl)porphyrin
MnTnOct-2-PyP^{5+}	Mn(III) *meso*-tetrakis(*N*-n-octylpyridinium-2-yl)porphyrin
MnTnOct-3-PyP^{5+}	Mn(III) *meso*-tetrakis(*N*-n-octylpyridinium-3-yl)porphyrin
MnTPhE-2-PyP^{5+}	Mn(III) *meso*-tetrakis (*N*-(2'-phenylethyl)pyridinium-2-yl)porphyrin
MnTnBuOE-2-PyP^{5+}	Mn(III) *meso*tetrakis(*N*-(2'-n-butoxyethyl)pyridinium-2-yl)porphyrin (BMX-001)
MnTnHexOE-2-PyP^{5+},	n(III) *meso*tetrakis(*N*-(2'-n-hexoxyethyl)pyridinium-2-yl)porphyrin
MnTE-2-PyPhP^{5+}	Mn(III) *meso*-tetrakis(phenyl-4'-(*N*-ethylpyridinium-2-yl))porphyrin
MnTPhE-2-PyP^{5+}	Mn(III) *meso*-tetrakis(N-(2′-phenylethyl)-pyridinium-2-yl)porphyrin
DMF	*N*,*N*-dimethylformamide
HFBA	heptafluorobutyric acid
$\boldsymbol{R_f}$	thin-layer chromatographic retention factor that presents the ratio between the solvent and compound path in 1:1:8=$KNO_{3(sat)}$ H_2O:H_2O:CH_3CN solvent system
$\boldsymbol{E_{1/2}}$	half-wave reduction potential
SOD	superoxide dismutase
NHE	normal hydrogen electrode; monodeprotonated form of ascorbic acid, HA^- (Asc) is a major species in aqueous solution at pH 7.8
Asc$^{\bullet}$	monodeprotonated ascorbyl radical; charges of MnPs are omitted in some Figures for simplicity

REFERENCES

1. Ashcraft KA, Boss M-K, Tovmasyan A, Choudhury KR, Fontanella AN, Young KH, Palmer GM, Birer SR, Landon CD, Park W, Das SK, Weitner T, Sheng H, Warner DS, Brizel DM, Spasojevic I, Batinic-Haberle I, Dewhirst MW. A novel manganese-porphyrin superoxide dismutase-mimetic widens the therapeutic margin in a pre-clinical head and neck cancer model. International Journal of Radiation Oncology*Biology*Physics. 2015
2. Weitzel DH, Tovmasyan A, Ashcraft KA, Rajic Z, Weitner T, Liu C, Li W, Buckley AF, Prasad MR, Young KH, Rodriguiz RM, Wetsel WC, Peters KB, Spasojevic I, Herndon JE 2nd, Batinic-Haberle I, Dewhirst MW. Radioprotection of the Brain White Matter by Mn(III) NButoxyethylpyridylporphyrin-Based Superoxide Dismutase Mimic MnTnBuOE-2-PyP5+. Mol Cancer Ther. 2015; 14:70–79. [PubMed: 25319393]
3. Gauter-Fleckenstein B, Fleckenstein K, Owzar K, Jiang C, Batinic-Haberle I, Vujaskovic Z. Comparison of two Mn porphyrin-based mimics of superoxide dismutase in pulmonary radioprotection. Free Radic Biol Med. 2008; 44:982–989. [PubMed: 18082148]
4. Gauter-Fleckenstein B, Fleckenstein K, Owzar K, Jiang C, Reboucas JS, Batinic-Haberle I, Vujaskovic Z. Early and late administration of MnTE-2-PyP5+ in mitigation and treatment of radiation-induced lung damage. Free Radic Biol Med. 2010; 48:1034–1043. [PubMed: 20096348]
5. Gridley DS, Makinde AY, Luo X, Rizvi A, Crapo JD, Dewhirst MW, Moeller BJ, Pearlstein RD, Slater JM. Radiation and a metalloporphyrin radioprotectant in a mouse prostate tumor model. Anticancer Res. 2007; 27:3101–3109. [PubMed: 17970050]
6. Moeller BJ, Batinic-Haberle I, Spasojevic I, Rabbani ZN, Anscher MS, Vujaskovic Z, Dewhirst MW. A manganese porphyrin superoxide dismutase mimetic enhances tumor radioresponsiveness. Int J Radiat Oncol Biol Phys. 2005; 63:545–552. [PubMed: 16168847]
7. Oberley-Deegan RE, Steffan JJ, Rove KO, Pate KM, Weaver MW, Spasojevic I, Frederick B, Raben D, Meacham RB, Crapo JD, Koul HK. The Antioxidant, MnTE-2-PyP, Prevents Side-Effects Incurred by Prostate Cancer Irradiation. PLoS One. 2012; 7:e44178. [PubMed: 22984473]
8. Batinic-Haberle I, Tovmasyan A, Roberts ER, Vujaskovic Z, Leong KW, Spasojevic I. SOD Therapeutics: Latest Insights into Their Structure-Activity Relationships and Impact on the Cellular Redox-Based Signaling Pathways. Antioxid Redox Signal. 2014; 20:2372–2415. [PubMed: 23875805]
9. Batinic-Haberle I, Tovmasyan A, Spasojevic I. An educational overview of the chemistry, biochemistry and therapeutic aspects of Mn porphyrins - From superoxide dismutation to H_2O_2-driven pathways. Redox Biol. 2015; 5:43–65. [PubMed: 25827425]
10. Jaramillo MC, Briehl MM, Batinic-Haberle I, Tome ME. Manganese (III) meso-tetrakis N-ethylpyridinium-2-yl porphyrin acts as a pro-oxidant to inhibit electron transport chain proteins, modulate bioenergetics, and enhance the response to chemotherapy in lymphoma cells. Free Radic Biol Med. 2015; 83:89–100. [PubMed: 25725417]
11. Jaramillo MC, Briehl MM, Crapo JD, Batinic-Haberle I, Tome ME. Manganese porphyrin, MnTE-2-PyP5+, Acts as a pro-oxidant to potentiate glucocorticoid-induced apoptosis in lymphoma cells. Free Radic Biol Med. 2012; 52:1272–1284. [PubMed: 22330065]
12. Guina T, Biasi F, Calfapietra S, Nano M, Poli G. Inflammatory and redox reactions in colorectal carcinogenesis. Ann N Y Acad Sci. 2015; 1340:95–103. [PubMed: 25727454]
13. Manda G, Isvoranu G, Comanescu MV, Manea A, Debelec Butuner B, Korkmaz KS. The redox biology network in cancer pathophysiology and therapeutics. Redox Biol. 2015; 5:347–357. [PubMed: 26122399]
14. Tong L, Chuang CC, Wu S, Zuo L. Reactive oxygen species in redox cancer therapy. Cancer Lett. 2015; 367:18–25. [PubMed: 26187782]
15. Gao MC, Jia XD, Wu QF, Cheng Y, Chen FR, Zhang J. Silencing Prx1 and/or Prx5 sensitizes human esophageal cancer cells to ionizing radiation and increases apoptosis via intracellular ROS accumulation. Acta Pharmacol Sin. 2011; 32:528–536. [PubMed: 21468086]
16. Kwei KA, Finch JS, Thompson EJ, Bowden GT. Transcriptional repression of catalase in mouse skin tumor progression. Neoplasia. 2004; 6:440–448. [PubMed: 15548352]

17. Nonn L, Berggren M, Powis G. Increased expression of mitochondrial peroxiredoxin-3 (thioredoxin peroxidase-2) protects cancer cells against hypoxia and drug-induced hydrogen peroxide-dependent apoptosis. Mol Cancer Res. 2003; 1:682–689. [PubMed: 12861054]
18. Sampson N, Koziel R, Zenzmaier C, Bubendorf L, Plas E, Jansen-Durr P, Berger P. ROS signaling by NOX4 drives fibroblast-to-myofibroblast differentiation in the diseased prostatic stroma. Mol Endocrinol. 2011; 25:503–515. [PubMed: 21273445]
19. Shen KK, Ji LL, Chen Y, Yu QM, Wang ZT. Influence of glutathione levels and activity of glutathione-related enzymes in the brains of tumor-bearing mice. Biosci Trends. 2011; 5:30–37. [PubMed: 21422598]
20. Sorokina LV, Solyanik GI, Pyatchanina TV. The evaluation of prooxidant and antioxidant state of two variants of lewis lung carcinoma: a comparative study. Exp Oncol. 2010; 32:249–253. [PubMed: 21270753]
21. Batinic-Haberle I, Spasojevic I, Tse HM, Tovmasyan A, Rajic Z, St Clair DK, Vujaskovic Z, Dewhirst MW, Piganelli JD. Design of Mn porphyrins for treating oxidative stress injuries and their redox-based regulation of cellular transcriptional activities. Amino Acids. 2012; 42:95–113. [PubMed: 20473774]
22. Hempel N, Carrico PM, Melendez JA. Manganese superoxide dismutase (Sod2) and redox-control of signaling events that drive metastasis. Anticancer Agents Med Chem. 2011; 11:191–201. [PubMed: 21434856]
23. Miriyala S, Spasojevic I, Tovmasyan A, Salvemini D, Vujaskovic Z, St Clair D, Batinic-Haberle I. Manganese superoxide dismutase, MnSOD and its mimics. Biochim Biophys Acta. 2012; 1822:794–814. [PubMed: 22198225]
24. Chaiswing L, Zhong W, Oberley TD. Distinct redox profiles of selected human prostate carcinoma cell lines: implications for rational design of redox therapy. Cancers (Basel). 2011; 3:3557–3584. [PubMed: 22163073]
25. Li JJ, Oberley LW, St Clair DK, Ridnour LA, Oberley TD. Phenotypic changes induced in human breast cancer cells by overexpression of manganese-containing superoxide dismutase. Oncogene. 1995; 10:1989–2000. [PubMed: 7761099]
26. Hempel N, Ye H, Abessi B, Mian B, Melendez JA. Altered redox status accompanies progression to metastatic human bladder cancer. Free Radic Biol Med. 2009; 46:42–50. [PubMed: 18930813]
27. Becuwe P, Ennen M, Klotz R, Barbieux C, Grandemange S. Manganese superoxide dismutase in breast cancer: from molecular mechanisms of gene regulation to biological and clinical significance. Free Radic Biol Med. 2014; 77:139–151. [PubMed: 25224035]
28. Miar A, Hevia D, Munoz-Cimadevilla H, Astudillo A, Velasco J, Sainz RM, Mayo JC. Manganese superoxide dismutase (SOD2/MnSOD)/catalase and SOD2/GPx1 ratios as biomarkers for tumor progression and metastasis in prostate, colon, and lung cancer. Free Radic Biol Med. 2015; 85:45–55. [PubMed: 25866291]
29. Kattan Z, Minig V, Leroy P, Dauca M, Becuwe P. Role of manganese superoxide dismutase on growth and invasive properties of human estrogen-independent breast cancer cells. Breast Cancer Res Treat. 2008; 108:203–215. [PubMed: 17473980]
30. Hsieh TC, Elangovan S, Wu JM. Differential suppression of proliferation in MCF-7 and MDAMB-231 breast cancer cells exposed to alpha-, gamma- and delta-tocotrienols is accompanied by altered expression of oxidative stress modulatory enzymes. Anticancer Res. 2010; 30:4169–4176. [PubMed: 21036737]
31. Ennen M, Minig V, Grandemange S, Touche N, Merlin JL, Besancenot V, Brunner E, Domenjoud L, Becuwe P. Regulation of the high basal expression of the manganese superoxide dismutase gene in aggressive breast cancer cells. Free Radic Biol Med. 2011; 50:1771–1779. [PubMed: 21419216]
32. Bueno-Janice J, Tovmasyan A, Batinic-Haberle I. Comprehensive study of GPx activity of different classes of redox-active therapeutics - implications for their therapeutic actions. Free Radic Biol Med Submitted. 2015
33. Evans MK, Tovmasyan A, Batinic-Haberle I, Devi GR. Mn porphyrin in combination with ascorbate acts as a pro-oxidant and mediates caspase-independent cancer cell death. Free Radic Biol Med. 2014; 68:302–314. [PubMed: 24334253]

34. Sheng H, Spasojevic I, Tse HM, Jung JY, Hong J, Zhang Z, Piganelli JD, Batinic-Haberle I, Warner DS. Neuroprotective Efficacy from a Lipophilic Redox-Modulating Mn(III) NHexylpyridylporphyrin, MnTnHex-2-PyP: Rodent Models of Ischemic Stroke and Subarachnoid Hemorrhage. J Pharmacol Exp Ther. 2011; 338:906–916. [PubMed: 21652782]
35. Sheng H, Yang W, Fukuda S, Tse HM, Paschen W, Johnson K, Batinic-Haberle I, Crapo JD, Pearlstein RD, Piganelli J, Warner DS. Long-term neuroprotection from a potent redox-modulating metalloporphyrin in the rat. Free Radic Biol Med. 2009; 47:917–923. [PubMed: 19631268]
36. Tse HM, Milton MJ, Piganelli JD. Mechanistic analysis of the immunomodulatory effects of a catalytic antioxidant on antigen-presenting cells: implication for their use in targeting oxidation-reduction reactions in innate immunity. Free Radic Biol Med. 2004; 36:233–247. [PubMed: 14744635]
37. Batinic-Haberle I, Rajic Z, Tovmasyan A, Reboucas JS, Ye X, Leong KW, Dewhirst MW, Vujaskovic Z, Benov L, Spasojevic I. Diverse functions of cationic Mn(III) N-substituted pyridylporphyrins, recognized as SOD mimics. Free Radic Biol Med. 2011; 51:1035–1053. [PubMed: 21616142]
38. Welsh JL, Wagner BA, van't Erve TJ, Zehr PS, Berg DJ, Halfdanarson TR, Yee NS, Bodeker KL, Du J, Roberts LJ 2nd, Drisko J, Levine M, Buettner GR, Cullen JJ. Pharmacological ascorbate with gemcitabine for the control of metastatic and node-positive pancreatic cancer (PACMAN): results from a phase I clinical trial. Cancer Chemother Pharmacol. 2013; 71:765–775. [PubMed: 23381814]
39. Batinic-Haberle, I.; Reboucas, JS.; Benov, L.; Spasojevic, I. Chemistry, biology and medical effects of water soluble metalloporphyrins.. In: Kadish, KM.; Smith, KM.; Guillard, R., editors. Handbook of Porphyrin Science. World Scientific; Singapore: 2011. p. 291-393.
40. Chen Q, Espey MG, Krishna MC, Mitchell JB, Corpe CP, Buettner GR, Shacter E, Levine M. Pharmacologic ascorbic acid concentrations selectively kill cancer cells: action as a pro-drug to deliver hydrogen peroxide to tissues. Proc Natl Acad Sci U S A. 2005; 102:13604–13609. [PubMed: 16157892]
41. Chen Q, Espey MG, Sun AY, Lee JH, Krishna MC, Shacter E, Choyke PL, Pooput C, Kirk KL, Buettner GR, Levine M. Ascorbate in pharmacologic concentrations selectively generates ascorbate radical and hydrogen peroxide in extracellular fluid in vivo. Proc Natl Acad Sci U S A. 2007; 104:8749–8754. [PubMed: 17502596]
42. Tovmasyan A, Carballal S, Ghazaryan R, Melikyan L, Weitner T, Maia CG, Reboucas JS, Radi R, Spasojevic I, Benov L, Batinic-Haberle I. Rational Design of Superoxide Dismutase (SOD) Mimics: The Evaluation of the Therapeutic Potential of New Cationic Mn Porphyrins with Linear and Cyclic Substituents. Inorg Chem. 2014; 53:11467–11483. [PubMed: 25333724]
43. Tovmasyan A, Carballal S, Ghazaryan R, Melikyan L, Weitner T, Maia CGC, Reboucas JS, Radi R, Spasojevic I, Benov L, Batinic-Haberle I. Rational Design of New Cationic Mn Porphyrins and Evaluation of Their Therapeutic Potential. Free Radic Biol Med. 2014; 76:S94.
44. Tovmasyan A, Roberts ERH, Yuliana Y, Haberle S, Boss M-K, Venkatraman TN, Lascola C, Dewhirst MW, Lam PYP, Benov L, Leong KW, Batinic-Haberle I. The Role of Ascorbate in Therapeutic Actions of Cationic Mn Porphyrin-Based SOD Mimics. Free Radic Biol Med. 2014; 76:S94–S95.
45. Ye X, Fels D, Tovmasyan A, Aird KM, Dedeugd C, Allensworth JL, Kos I, Park W, Spasojevic I, Devi GR, Dewhirst MW, Leong KW, Batinic-Haberle I. Cytotoxic effects of Mn(III) N-alkylpyridylporphyrins in the presence of cellular reductant, ascorbate. Free Radic Res. 2011; 45:1289–1306. [PubMed: 21859376]
46. Tovmasyan A, Bueno-Janice J, Boss M-K, Weitzel DH, Sampaio RS, Spasojevic I, Dewhirst MW, Batinic-Haberle I. Mn porphyrin-based SOD mimic and vitamin C enhance radiation-induced tumor growth inhibition. Free Radic Biol Med Submitted. 2015
47. Yulyana Y, Tovmasyan A, Ho IAW, Sia KC, P. NJ, H. NW, Guo CM, Hui KM, Batinic-Haberle I, Lam P. Redox-active Mn porphyrin enhances carbenoxolone-mediated TRAIL-induced apoptosis in glioblastoma multiforme. Stem Cell Rev Rep. 2015

48. Cieslak JA, Strother RK, Rawal M, Du J, Doskey CM, Schroeder SR, Button A, Wagner BA, Buettner GR, Cullen JJ. Manganoporphyrins and ascorbate enhance gemcitabine cytotoxicity in pancreatic cancer. Free Radic Biol Med. 2015; 83:227–237. [PubMed: 25725418]
49. Tian J, Peehl DM, Knox SJ. Metalloporphyrin synergizes with ascorbic acid to inhibit cancer cell growth through fenton chemistry. Cancer Biother Radiopharm. 2010; 25:439–448. [PubMed: 20735206]
50. Tovmasyan A, Weitner T, Sheng H, Lu M, Rajic Z, Warner DS, Spasojevic I, Reboucas JS, Benov L, Batinic-Haberle I. Differential Coordination Demands in Fe versus Mn Water-Soluble Cationic Metalloporphyrins Translate into Remarkably Different Aqueous Redox Chemistry and Biology. Inorg Chem. 2013; 52:5677–5691. [PubMed: 23646875]
51. Rajic Z, Tovmasyan A, Spasojevic I, Sheng H, Lu M, Li AM, Gralla EB, Warner DS, Benov L, Batinic-Haberle I. A new SOD mimic, Mn(III) ortho N-butoxyethylpyridylporphyrin, combines superb potency and lipophilicity with low toxicity. Free Radic Biol Med. 2012; 52:1828–1834. [PubMed: 22336516]
52. Reboucas JS, Kos I, Vujaskovic Z, Batinic-Haberle I. Determination of residual manganese in Mn porphyrin-based superoxide dismutase (SOD) and peroxynitrite reductase mimics. J Pharm Biomed Anal. 2009; 50:1088–1091. [PubMed: 19660888]
53. Benson BB, Krause D Jr. The Concentration and Isotopic Fractionation of Gases Dissolved in Freshwater in Equilibrium with the Atmosphere. 1. Oxygen. Limnology and Oceanography. 1980; 25:662–671.
54. Tovmasyan A, Maia CG, Weitner T, Carballal S, Sampaio RS, Lieb D, Ghazaryan R, Ivanovic-Burmazovic I, Ferrer-Sueta G, Radi R, Reboucas JS, Spasojevic I, Benov L, Batinic-Haberle I. A comprehensive evaluation of catalase-like activity of different classes of redox-active therapeutics. Free Radic Biol Med. 2015; 86:308–321. [PubMed: 26026699]
55. Tovmasyan AG, Rajic Z, Spasojevic I, Reboucas JS, Chen X, Salvemini D, Sheng H, Warner DS, Benov L, Batinic-Haberle I. Methoxy-derivatization of alkyl chains increases the in vivo efficacy of cationic Mn porphyrins. Synthesis, characterization, SOD-like activity, and SOD-deficient E. coli study of meta Mn(III) N-methoxyalkylpyridylporphyrins. Dalton Trans. 2011; 40:4111–4121. [PubMed: 21384047]
56. Mouraviev V, Venkatraman T, Tovmasyan A, Kimura M, Tsivian M, Mouravieva V, Polascik T, Wang H, Amrhein TJ, Batinic-Haberle I, Lascola C. Mn Porphryins as Novel Molecular MRI Contrast Agents. J Endourol. 2012
57. Ezzeddine R, Al-Banaw A, Tovmasyan A, Craik JD, Batinic-Haberle I, Benov LT. Effect of molecular characteristics on cellular uptake, subcellular localization, and phototoxicity of Zn(II) N-alkylpyridylporphyrins. J Biol Chem. 2013; 288:36579–36588. [PubMed: 24214973]
58. Kos I, Benov L, Spasojevic I, Reboucas JS, Batinic-Haberle I. High lipophilicity of meta Mn(III) N-alkylpyridylporphyrin-based superoxide dismutase mimics compensates for their lower antioxidant potency and makes them as effective as ortho analogues in protecting superoxide dismutase-deficient Escherichia coli. J Med Chem. 2009; 52:7868–7872. [PubMed: 19954250]
59. Lowry OH, Rosebrough NJ, Farr AL, Randall RJ. Protein measurement with the Folin phenol reagent. J Biol Chem. 1951; 193:265–275. [PubMed: 14907713]
60. Jones DP, Liang Y. Measuring the poise of thiol/disulfide couples in vivo. Free Radical Biology and Medicine. 2009; 47:1329–1338. [PubMed: 19715755]
61. Jones DP, Carlson JL, Mody VC, Cai J, Lynn MJ, Sternberg P. Redox state of glutathione in human plasma. Free Radic Biol Med. 2000; 28:625–635. [PubMed: 10719244]
62. Kirlin WG, Cai J, Thompson SA, Diaz D, Kavanagh TJ, Jones DP. Glutathione redox potential in response to differentiation and enzyme inducers. Free Radic Biol Med. 1999; 27:1208–1218. [PubMed: 10641713]
63. Chandler JD, Nichols DP, Nick JA, Hondal RJ, Day BJ. Selective metabolism of hypothiocyanous acid by mammalian thioredoxin reductase promotes lung innate immunity and antioxidant defense. J Biol Chem. 2013; 288:18421–18428. [PubMed: 23629660]
64. Chen Q, Espey MG, Sun AY, Pooput C, Kirk KL, Krishna MC, Khosh DB, Drisko J, Levine M. Pharmacologic doses of ascorbate act as a prooxidant and decrease growth of aggressive tumor xenografts in mice. Proc Natl Acad Sci U S A. 2008; 105:11105–11109. [PubMed: 18678913]

65. Weitner T, Kos I, Sheng H, Tovmasyan A, Reboucas JS, Fan P, Warner DS, Vujaskovic Z, Batinic-Haberle I, Spasojevic I. Comprehensive pharmacokinetic studies and oral bioavailability of two Mn porphyrin-based SOD mimics, MnTE-2-PyP(5+) and MnTnHex-2-PyP(5+). Free Radic Biol Med. 2013; 58:73–80. [PubMed: 23328731]

66. Batinic-Haberle I, Reboucas JS, Spasojevic I. Superoxide dismutase mimics: chemistry, pharmacology, and therapeutic potential. Antioxid Redox Signal. 2010; 13:877–918. [PubMed: 20095865]

67. Tovmasyan A, Sheng H, Weitner T, Arulpragasam A, Lu M, Warner DS, Vujaskovic Z, Spasojevic I, Batinic-Haberle I. Design, mechanism of action, bioavailability and therapeutic effects of mn porphyrin-based redox modulators. Med Princ Pract. 2013; 22:103–130. [PubMed: 23075911]

68. Ferrer-Sueta G, Vitturi D, Batinic-Haberle I, Fridovich I, Goldstein S, Czapski G, Radi R. Reactions of manganese porphyrins with peroxynitrite and carbonate radical anion. J Biol Chem. 2003; 278:27432–27438. [PubMed: 12700236]

69. Ye X, Fels D, Dedeugd C. The in vitro Cytotoxic Effects of Mn(III) alkylpyridylporphyrin/ascorbate system on 8 tumor cell lines. Free Radic Biol Med. 2009; 47:S137.

70. Zhao Y, Chaiswing L, Oberley TD, Batinic-Haberle I, St Clair W, Epstein CJ, St Clair D. A mechanism-based antioxidant approach for the reduction of skin carcinogenesis. Cancer Res. 2005; 65:1401–1405. [PubMed: 15735027]

71. Holley AK, Xu Y, Noel T, Bakthavatchalu V, Batinic-Haberle I, St Clair DK. Manganese superoxide dismutase-mediated inside-out signaling in HaCaT human keratinocytes and SKH-1 mouse skin. Antioxid Redox Signal. 2014; 20:2347–2360. [PubMed: 24635018]

72. Zhao Y, Miriyala S, Miao L, Mitov M, Schnell D, Dhar SK, Cai J, Klein JB, Sultana R, Butterfield DA, Vore M, Batinic-Haberle I, Bondada S, St Clair DK. Redox proteomic identification of HNE-bound mitochondrial proteins in cardiac tissues reveals a systemic effect on energy metabolism after doxorubicin treatment. Free Radic Biol Med. 2014; 72:55–65. [PubMed: 24632380]

73. Miriyala S, Thippakorn C, Chaiswing L, Xu Y, Noel T, Tovmasyan A, Batinic-Haberle I, Kooi C, Chi W, Abdel L, Reda H, Oberley T, Prachayasittikul V, St Clair D. 4-hydroxy-2-nonenal triggers AIFM2-mediated retrograde signaling by activating its translocation and function switching. Free Radic Biol Med In Revision. 2015

74. Tovmasyan A, Weitner T, Jaramillo M, Wedmann R, Roberts ERH, Leong KW, Filipovic M, Ivanovic-Burmazovic I, Benov L, Tome ME, Batinic-Haberle I. We Have Come a Long Way with Mn Porphyrins: from Superoxide Dismutation to H2O2-Driven Pathways. Free Radic Biol Med. 2013; 65:S133.

75. Verrax J, Beck R, Dejeans N, Glorieux C, Sid B, Pedrosa RC, Benites J, Vasquez D, Valderrama JA, Calderon PB. Redox-active quinones and ascorbate: an innovative cancer therapy that exploits the vulnerability of cancer cells to oxidative stress. Anticancer Agents Med Chem. 2011; 11:213–221. [PubMed: 21395522]

76. Beck R, Pedrosa RC, Dejeans N, Glorieux C, Leveque P, Gallez B, Taper H, Eeckhoudt S, Knoops L, Calderon PB, Verrax J. Ascorbate/menadione-induced oxidative stress kills cancer cells that express normal or mutated forms of the oncogenic protein Bcr-Abl. An in vitro and in vivo mechanistic study. Invest New Drugs. 2011; 29:891–900. [PubMed: 20454833]

77. Beck R, Verrax J, Gonze T, Zappone M, Pedrosa RC, Taper H, Feron O, Calderon PB. Hsp90 cleavage by an oxidative stress leads to its client proteins degradation and cancer cell death. Biochem Pharmacol. 2009; 77:375–383. [PubMed: 19014912]

78. Aime S, Anelli L, Botta M, Brocchetta M, Canton S, Fedeli F, Gianolio E, Terreno E. Relaxometric evaluation of novel manganese(II) complexes for application as contrast agents in magnetic resonance imaging. J Biol Inorg Chem. 2002; 7:58–67. [PubMed: 11862541]

79. Koenig SH, Baglin C, Brown RD 3rd, Brewer CF. Magnetic field dependence of solvent proton relaxation induced by Gd3+ and Mn2+ complexes. Magn Reson Med. 1984; 1:496–501. [PubMed: 6443784]

80. Koenig SH, Brown RD 3rd, Spiller M. The anomalous relaxivity of Mn3+ (TPPS4). Magn Reson Med. 1987; 4:252–260. [PubMed: 3574059]

81. Batinić-Haberle I, Spasojević I, Hambright P, Benov L, Crumbliss AL, Fridovich I. Relationship among Redox Potentials, Proton Dissociation Constants of Pyrrolic Nitrogens, and in Vivo and in Vitro Superoxide Dismutating Activities of Manganese(III) and Iron(III) Water-Soluble Porphyrins. Inorg Chem. 1999; 38:4011–4022.

82. Budimir A, Kalmar J, Fabian I, Lente G, Banyai I, Batinic-Haberle I, Birus M. Water exchange rates of water-soluble manganese(III) porphyrins of therapeutical potential. Dalton Trans. 2010; 39:4405–4410. [PubMed: 20422097]

83. Kellar KE, Foster N. Relaxation enhancement of water protons by manganese(III) porphyrins: influence of porphyrin aggregation. Inorganic Chemistry. 1992; 31:1353–1359.

84. Mercier GA Jr. On the molecular spin density and the electrostatic potential as determinants of the relaxivity of metalloporphyrins. Magn Reson Imaging. 1995; 13:807–817. [PubMed: 8544652]

85. Schmiedl UP, Nelson JA, Starr FL, Schmidt R. Hepatic contrast-enhancing properties of manganese-mesoporphyrin and manganese-TPPS4. A comparative magnetic resonance imaging study in rats. Invest Radiol. 1992; 27:536–542. [PubMed: 1644554]

86. Rawal M, Schroeder SR, Wagner BA, Cushing CM, Welsh JL, Button AM, Du J, Sibenaller ZA, Buettner GR, Cullen JJ. Manganoporphyrins Increase Ascorbate-Induced Cytotoxicity by Enhancing H2O2 Generation. Cancer Res. 2013; 73:5232–5241. [PubMed: 23764544]

87. Moeller BJ, Cao Y, Li CY, Dewhirst MW. Radiation activates HIF-1 to regulate vascular radiosensitivity in tumors: role of reoxygenation, free radicals, and stress granules. Cancer Cell. 2004; 5:429–441. [PubMed: 15144951]

88. Agus DB, Vera JC, Golde DW. Stromal cell oxidation: a mechanism by which tumors obtain vitamin C. Cancer Res. 1999; 59:4555–4558. [PubMed: 10493506]

89. Jaramillo MC, Frye JB, Crapo JD, Briehl MM, Tome ME. Increased manganese superoxide dismutase expression or treatment with manganese porphyrin potentiates dexamethasone-induced apoptosis in lymphoma cells. Cancer Res. 2009; 69:5450–5457. [PubMed: 19549914]

90. Batinic-Haberle I, Rajic Z, Benov L. A combination of two antioxidants (an SOD mimic and ascorbate) produces a pro-oxidative effect forcing Escherichia coli to adapt via induction of oxyR regulon. Anticancer Agents Med Chem. 2011; 11:329–340. [PubMed: 21355843]

91. Landolt H, Langemann H, Probst A, Gratzl O. Levels of water-soluble antioxidants in astrocytoma and in adjacent tumor-free tissue. J Neurooncol. 1994; 21:127–133. [PubMed: 7861188]

92. Padayatty SJ, Sun H, Wang Y, Riordan HD, Hewitt SM, Katz A, Wesley RA, Levine M. Vitamin C pharmacokinetics: implications for oral and intravenous use. Ann Intern Med. 2004; 140:533–537. [PubMed: 15068981]

93. Batinic-Haberle I, Keir ST, Rajic Z, Tovmasyan A, Spasojevic I, Dewhirst MW, Bigner DD. Glioma growth suppression via modulation of cellular redox status by a lipophilic Mn porphyrin. Mid-Winter SPORE Meeting.:31-32. 2011

94. Batinic-Haberle I, Tovmasyan A, Weitner T, Rajic Z, Keir ST, Huang T-T, Leu D, Weitzel DH, Beausejour CM, Miriyala S, Roberts ERH, Dewhirst MW, Clair DS, Leong KW, Spasojevic I, Piganelli J, Tome M. Mechanistic Considerations of the Therapeutic Effects of Mn Porphyrins, Commonly Regarded as SOD Mimics, in Anticancer Therapy: Lessons from Brain and Lymphoma Studies. Free Radic Biol Med. 2013; 65:S120–S121.

95. Du J, Cieslak JA 3rd, Welsh JL, Sibenaller ZA, Allen BG, Wagner BA, Kalen AL, Doskey CM, Strother RK, Button AM, Mott SL, Smith B, Tsai S, Mezhir J, Goswami PC, Spitz DR, Buettner GR, Cullen JJ. Pharmacological Ascorbate Radiosensitizes Pancreatic Cancer. Cancer Res. 2015

HIGHLIGHTS

- Mn porphyrins (MnPs) catalyze ascorbate (Asc) oxidation, thereby producing H_2O_2
- MnP-driven H_2O_2 production depends on the Mn^{III}/Mn^{II} reduction potential
- The potency of MnP in catalyzing Asc oxidation correlates with the cytotoxicity induced by MnP/Asc
- MnP/Asc is cytotoxic to 3 breast cancer cell lines, but not to non-cancerous breast epithelial cells
- MnP/Asc suppresses tumor growth in a mouse flank model
- MnP accumulates to much higher levels in tumor than normal tissue

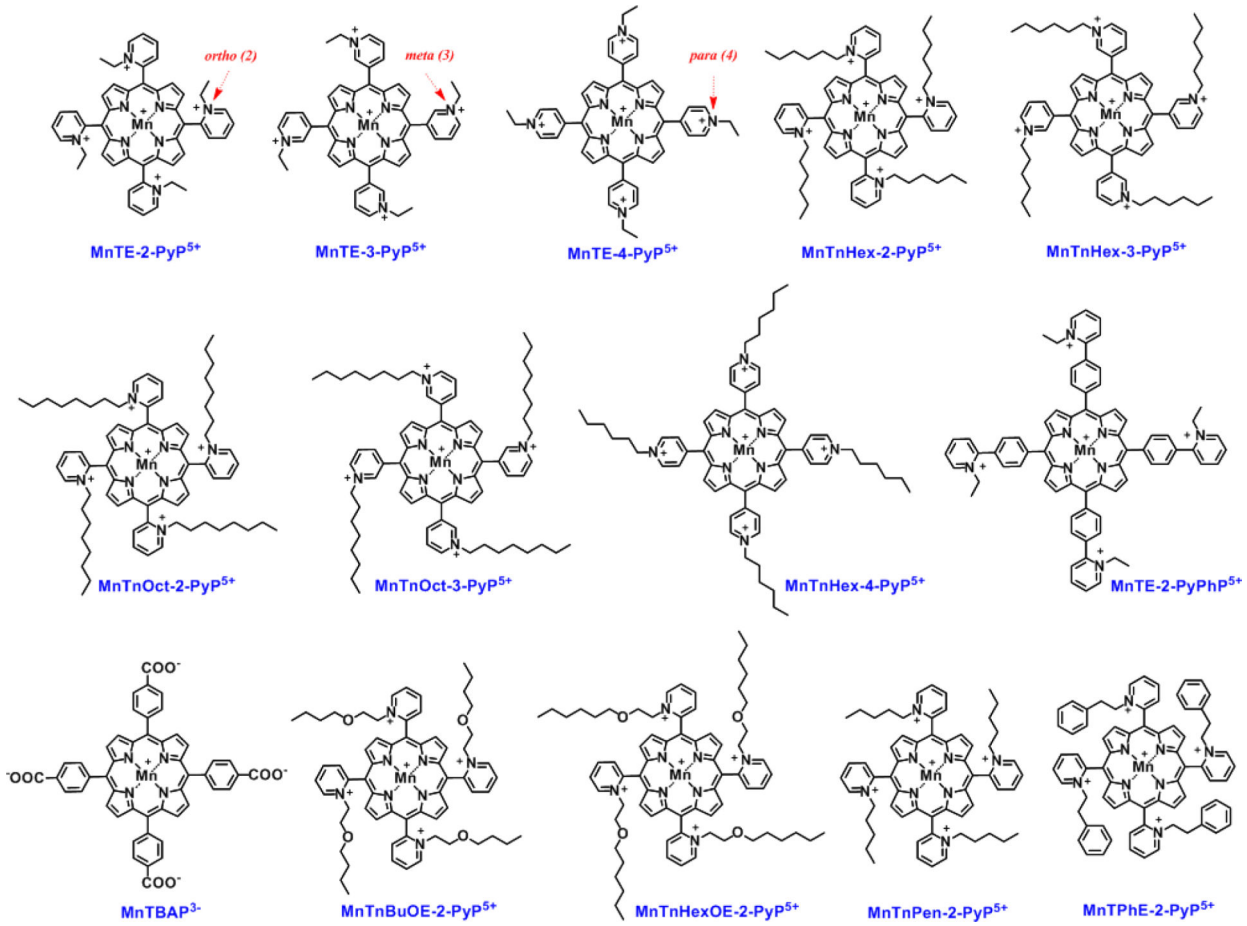

Figure 1. Structures of the Mn(III) porphyrins whose ability to catalyze ascorbate oxidation was assessed herein

Except $MnTBAP^{3-}$ and $MnTE\text{-}2\text{-}PyPhP^{5+}$, all MnPs studied are SOD mimics of various potency with log $k_{cat}(O_2^{\cdot-})$ ranging from 6.53 to 7.92. Their SOD-like activity is controlled by the cationic *ortho*, *meta* and *para* (2, 3 or 4, respectfully) electron-withdrawing pyridyl (Py) nitrogens in the vicinity of the metal site. This in turns controls thermodynamics and kinetics (electrostatics, sterics, electronics) of not only catalysis of $O_2^{\cdot-}$ dismutation, but of reactions of MnPs with other reactive species such as $ONOO^-$, H_2O_2, RS^- and cellular reductants, GSH, ascorbate and tetrahydrobiopterin [8, 9].

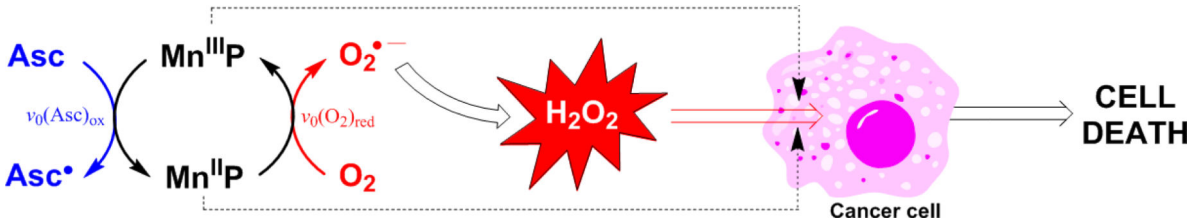

Figure 2. Catalysis of ascorbate oxidation by MnP leads to H_2O_2 production

MnP cycles between +3 ($Mn^{III}P$) and +2 ($Mn^{II}P$) oxidation states while oxidizing ascorbate to ascorbyl radical, Asc•. The re-oxidation of $Mn^{II}P$ with oxygen closes the catalytic cycle, giving rise to superoxide, $O_2^{\cdot -}$ which readily undergoes dismutation to H_2O_2. MnP subsequently uses H_2O_2 to suppress cellular transcriptional pathways such as NF-κB, AP-1 and SP-1. The magnitude of the outcome is dependent upon the levels of MnPs and H_2O_2. Based on our data and those of others, both Mn porphyrin (this work and ref [45]) and H_2O_2 [10-14] are at higher levels in tumor than in normal tissue. Consequently, suppression of tumor growth accompanied by normal tissue healing was seen herein and elsewhere [1, 2, 8-11, 39, 66, 67]. Asc and Asc• describe the predominant monodeprotonated ascorbic acid (HA^-) and deprotonated ascorbyl radical at pH 7.8, respectively. The catalysis of ascorbate oxidation is characterized in this work with initial rates of ascorbate oxidation ($v_0(Asc)_{ox}$) and oxygen consumption/reduction ($v_0(O_2)_{red}$).

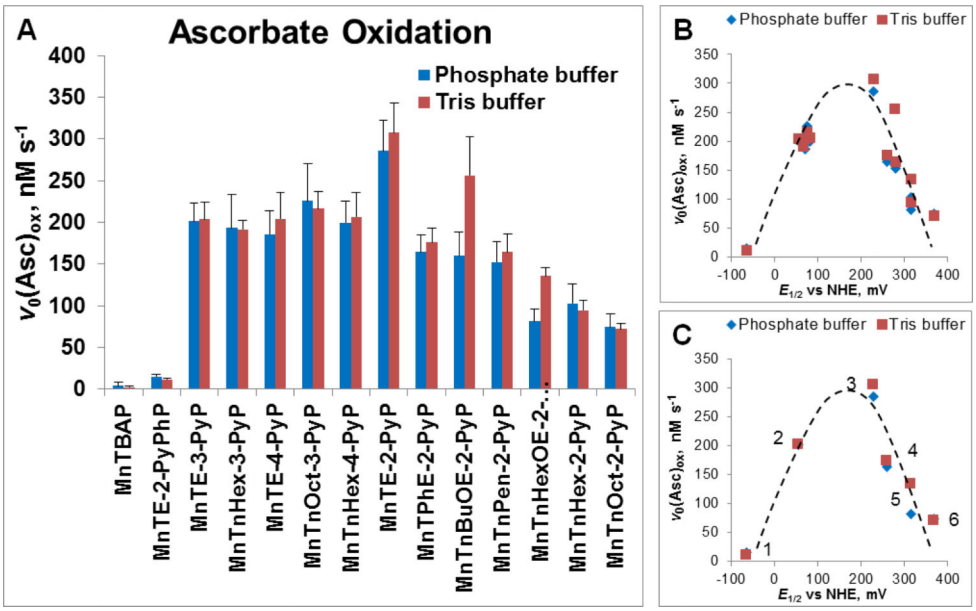

Figure 3. Ability of MnPs to catalyze ascorbate oxidation as assessed spectrophotometrically *via* determination of initial rates of ascorbate oxidation, v_0 (Asc)$_{ox}$

(A) The v_0(Asc)$_{ox}$ was measured for various MnPs which differ vastly with respect to their redox properties, lipophilicity/bioavailability, polarity, size and bulkiness. Initial rates were determined with 5 μM MnP, 5 mM EDTA and 0.15 mM sodium ascorbate under aerobic conditions at (25 ± 1)^{0}C and at pH 7.8 maintained with either 0.05 M potassium phosphate or Tris buffer. (**B**) Relationship between v_0(Asc)$_{ox}$ and $E_{1/2}$ is of bell-shape. (**C**) Six cationic MnPs with the $E_{1/2}$ ranging from −65 to +340 mV *vs* NHE are plotted: (#1) MnTE-2-PyPhP^{5+}, (#2) MnTE-3-PyP^{5+}, (#3) MnTE-2-PyP^{5+}, (#4) MnTPhE-2-PyP^{5+}, (#5), MnTnHexOE-2-PyP^{5+}, and (#6) MnTnOct-2-PyP^{5+}.

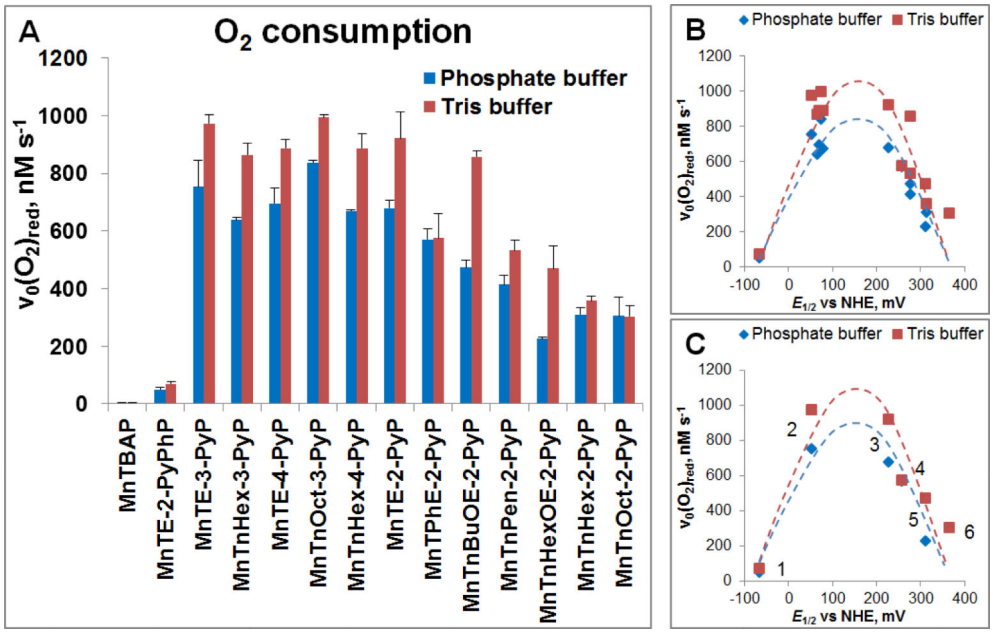

Figure 4. Ability of MnP to catalyze ascorbate oxidation as assessed electrochemically via determination of initial rates of oxygen reduction

(**A**) MnP/Asc cycled under aerobic conditions, whereby oxygen is consumed through reduction to superoxide (**Figure 2**). The $v_0(O_2)_{red}$ was measured with 10 μM MnP and 1 mM Asc under aerobic conditions ($[O_2]$ = 0.255 mM) at (25 ± 1)^{0}C and at pH 7.8 maintained with either 0.05 M phosphate or Tris buffer. (**B**) Relationship between $v_0(O_2)_{red}$ and $E_{1/2}$ is of bell-shape. (**C**) Six cationic MnPs with $E_{1/2}$ ranging from −65 to +340 mV *vs* NHE are plotted: (#1) MnTE-2-PyPhP^{5+}, (#2) MnTE-3-PyP^{5+}, (#3) MnTE-2-PyP^{5+}, (#4) MnTPhE-2-PyP^{5+}, (#5), MnTnHexOE-2-PyP^{5+}, and (#6) MnTnOct-2-PyP^{5+}.

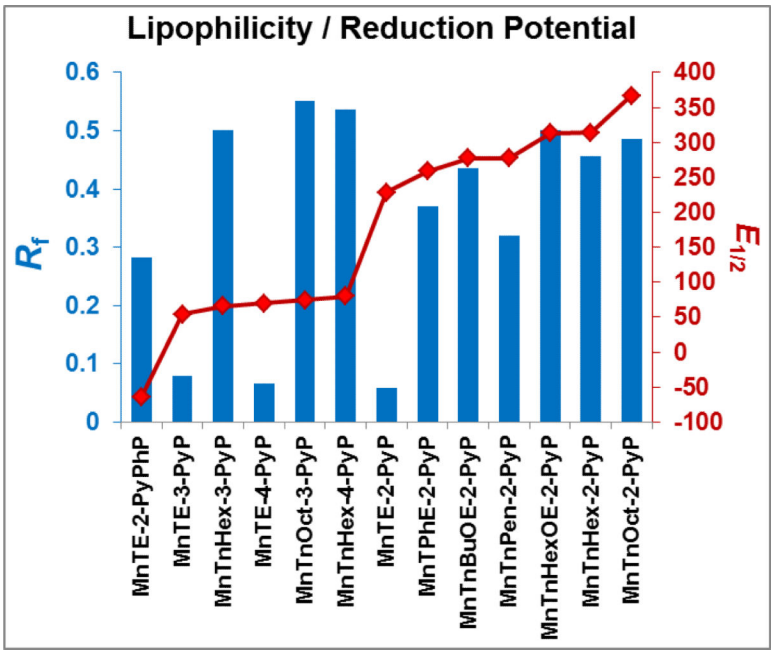

Figure 5. Lipophilicity of MnPs expressed in terms of chromatographic retention factor, R_f (blue bars)

R_f presents ratio of compound path to solvent path on silica gel plastic plates with 1:1:8=$KNO_{3(sat)}$ H_2O:H_2O:CH_3CN as solvent. MnPs with low, medium, and high lipophilicity were included in this study. Their $E_{1/2}$ values (marked in red) range from −65 to +340 mV *vs* NHE, and (illustrate the diversity of MnPs investigated in this study.

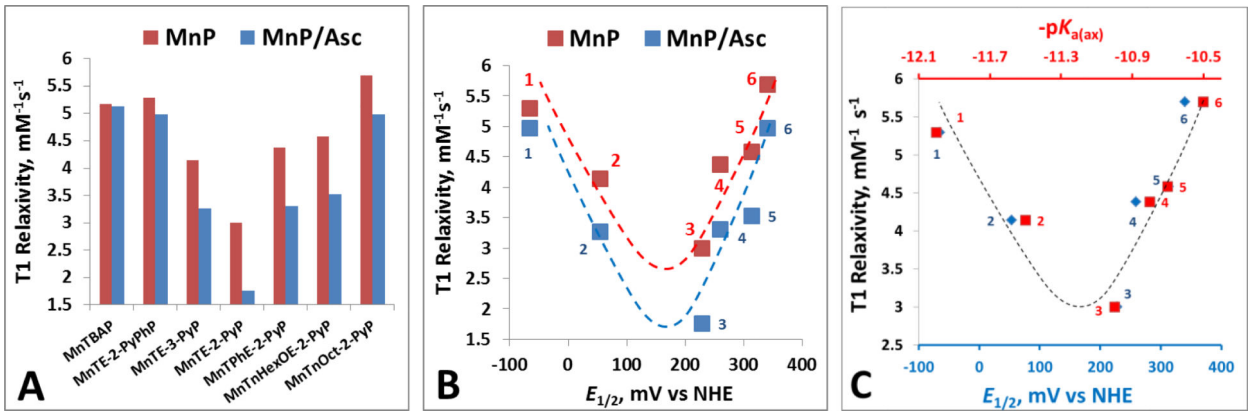

Figure 6. MRI studies of MnPs

MnPs were 0.1 mM and ascorbate was 5 mM in 0.05 M phosphate buffer, pH 7.8, (25±1)^{0}C. The T1 relaxivity measurements were carried out immediately after ascorbate addition. **(A)** T1 relaxivity values in the absence and presence of ascorbate, Asc, are plotted for different MnPs. **(B)** T1 relaxivity values in the presence and absence of ascorbate are plotted versus metal-centered reduction potential, $E_{1/2}$. **(C)** T1 relaxivity values are plotted versus $E_{1/2}$ and p$K_{a(ax)}$. The following porphyrins are plotted in **(B)** and **(C):** (#1) MnTE-2-PyPhP^{5+}, (#2) MnTE-3-PyP^{5+}, (#3) MnTE-2-PyP^{5+}, (#4) MnTPhE-2-PyP^{5+}, (#5), MnTnHexOE-2-PyP^{5+}, and (#6) MnTnOct-2-PyP^{5+}.

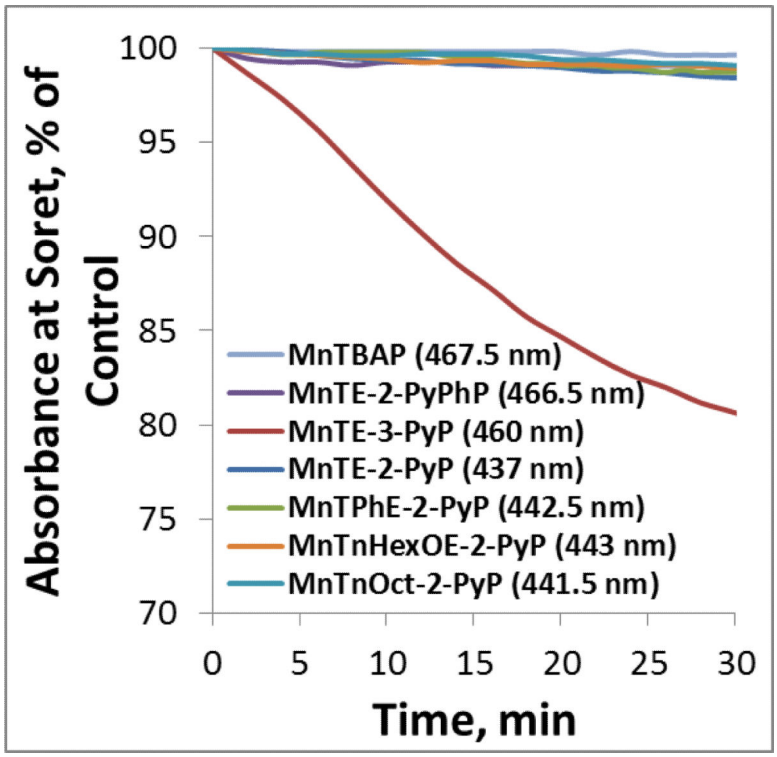

Figure 7. Stabilities of MnPs towards Asc-mediated oxidative degradation

5 μM MnPs were incubated with 1 mM ascorbate in the 0.05 M Tris buffer at pH 7.8. The H_2O_2, which is produced during the MnP/Asc cycling, accumulates in the solution and leads to MnP degradation The stability of MnPs was followed spectrophotometrically at Soret band which corresponds either to Mn +3 (Mn^{III}TE-3-PyP^{5+} and Mn^{II}TE-2-$PyPhP^{4+}$), or +2 oxidation state (Mn^{II}TE-2-PyP^{4+}, MnTnOct-2-PyP^{5+}, MnTnHexOE-2-PyP^{5+} Mn^{II}TPhE-2-PyP^{4+}) oxidation states. Mn^{III}TE-3-PyP^{5+} is hardly reducible under aerobic conditions and once reduced re-oxidizes to Mn +3 oxidation state order of magnitude faster than MnTE-2-PyP^{5+} [33].

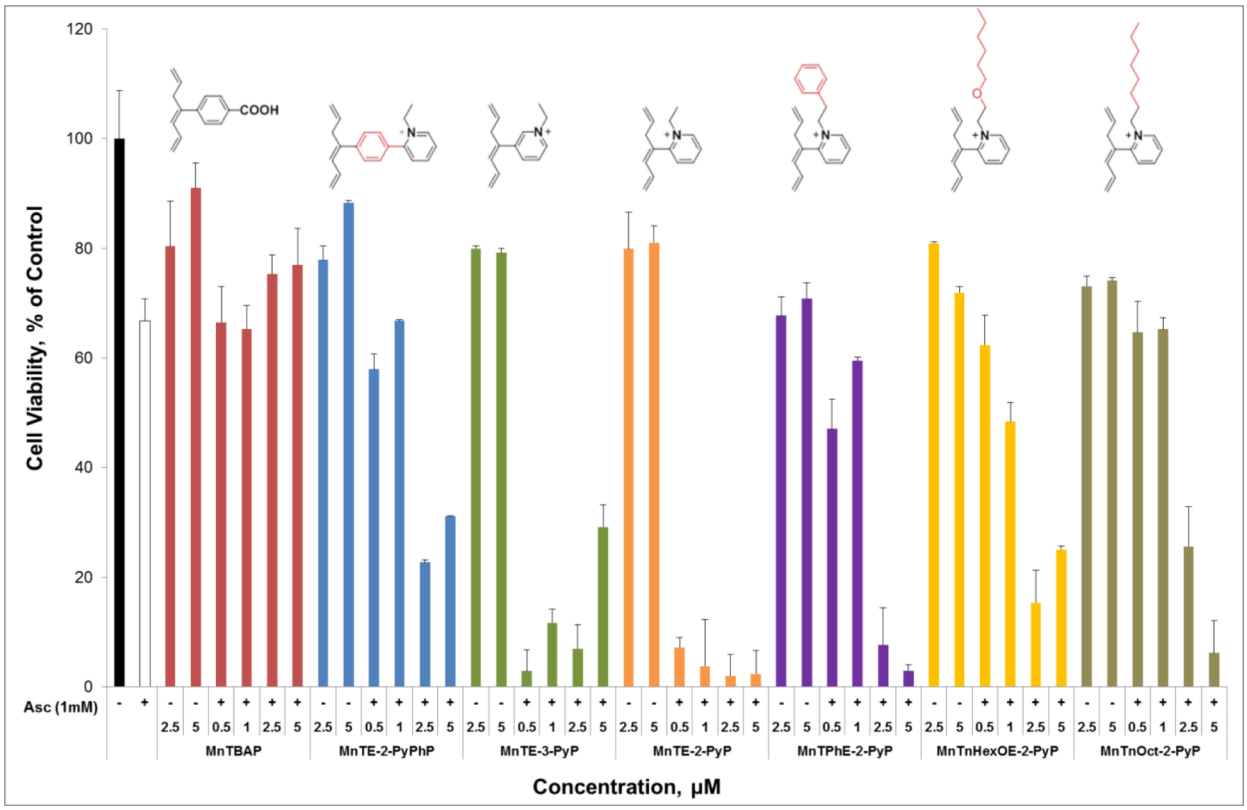

Figure 8. Cytotoxicity of MnP/Asc to 4T1 mouse breast cancer cell line

Cells were incubated with MnP at various concentrations in the absence and presence of 1 mM ascorbate for 24 hours, followed by MTT-based assessment of cell viability.

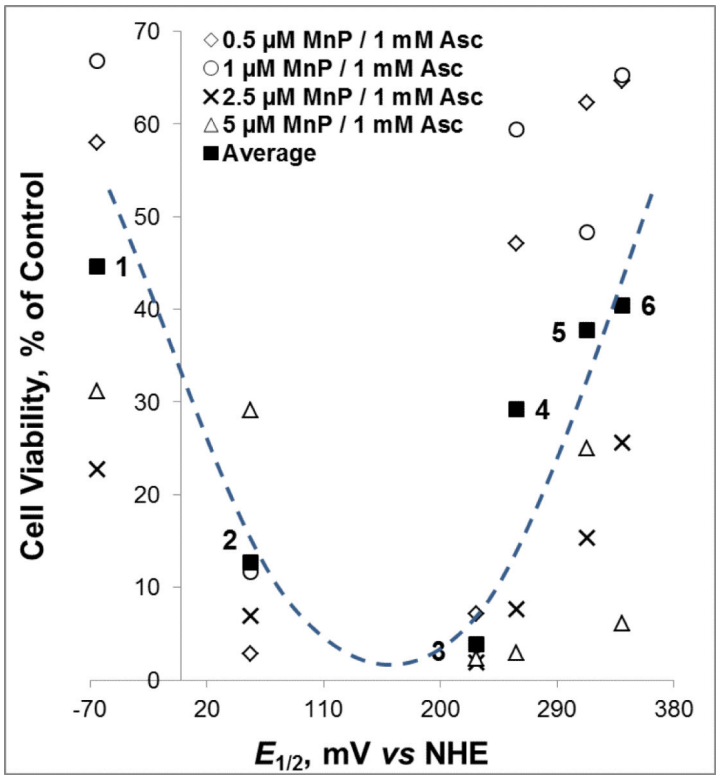

Figure 9. Role of the redox properties of MnPs (described by metal-centered reduction potential, $E_{1/2}$) in the cytotoxicity of MnP/Asc to 4T1 mouse breast cancer cell line

Cell viability data are taken from **Figure 8**. The bell-shape relationship between the cell viability and $E_{1/2}$ correlates well with the structure-activity relationship observed between $v_0(\text{Asc})_{ox}$ and $E_{1/2}$ (**Figure 3)**: the higher is $E_{1/2}$, the higher is the $v_0(\text{Asc})_{ox}$. In turn the higher is the rate of H_2O_2 production and the higher is the cytotoxicity induced by MnP/Asc system. While the bulky compounds (MnTPhE-2-PyP^{5+}, MnTnHexOE-2-PyP^{5+} and MnTnOct-2-PyP^{5+}) have favorable redox properties, the approach of ascorbate towards their Mn site is hindered. In turn the production of H_2O_2 and the cytotoxicity is diminished relative to a smaller molecule of MnTE-2-PyP^{5+}, giving rise to bell shape behavior. Reduced cellular uptake of such bulky MnPs may also play a role. The following porphyrins are plotted: (#1) MnTE-2-PyPhP^{5+}, (#2) MnTE-3-PyP^{5+}, (#3) MnTE-2-PyP^{5+}, (#4) MnTPhE-2-PyP^{5+}, (#5), MnTnHexOE-2-PyP^{5+} and (#6) MnTnOct-2-PyP^{5+}.

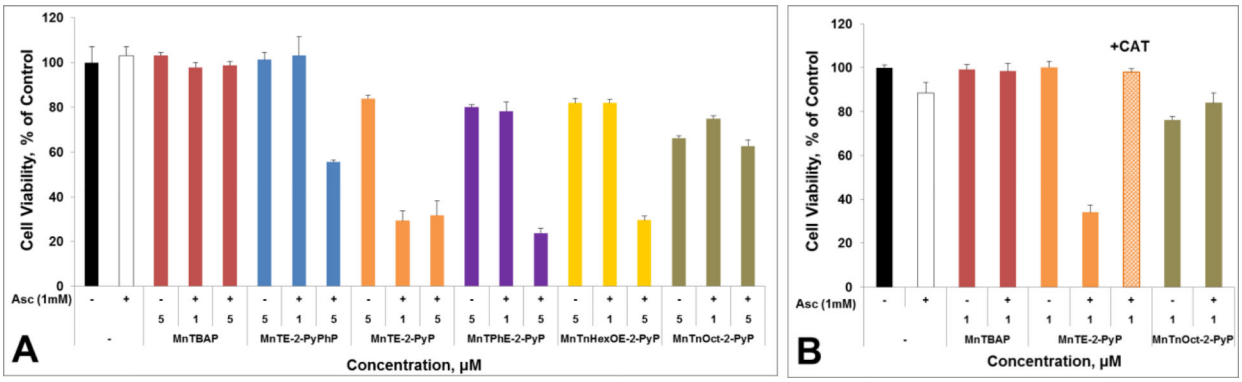

Figure 10. Cytotoxicity of MnP/Asc to human breast cancer MCF-7 (A) and MDA-MB-231 (B) cell lines

Cells were incubated with MnP +/− ascorbate at given concentrations for 24 hours. Viability was determined by the MTT assay. The effect of catalase was exemplified with MDA-MB-231. Exogenous catalase (1000 units/mL) fully blocked the cytotoxic effect of MnTE-2-PyP^{5+}/Asc **(B),** indicating that H_2O_2 produced in medium is primarily responsible for the observed cytotoxicity.

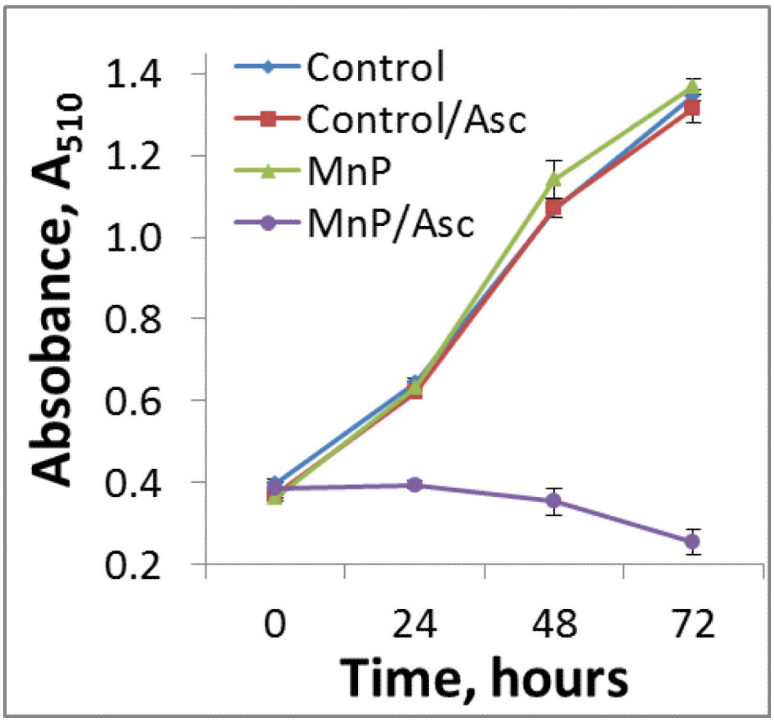

Figure 11. MnTE-2-PyP^{5+}/Asc inhibits proliferation of human breast cancer cells

MCF-7 cells were incubated with either 1 (data not shown) or 5 μM MnTE-2-PyP^{5+} and 1 mM ascorbate. Complete inhibition of proliferation by MnP/Asc under identical conditions was also seen with 4T1 mouse breast cancer cells. MnTE-2-PyP^{5+} was chosen for cell proliferation and mouse study. When combined with ascorbate **(i)** it has the largest ability to catalyze ascorbate oxidation, and **(ii)** exhibited the largest cytotoxicity towards 3 different cancer cell lines.

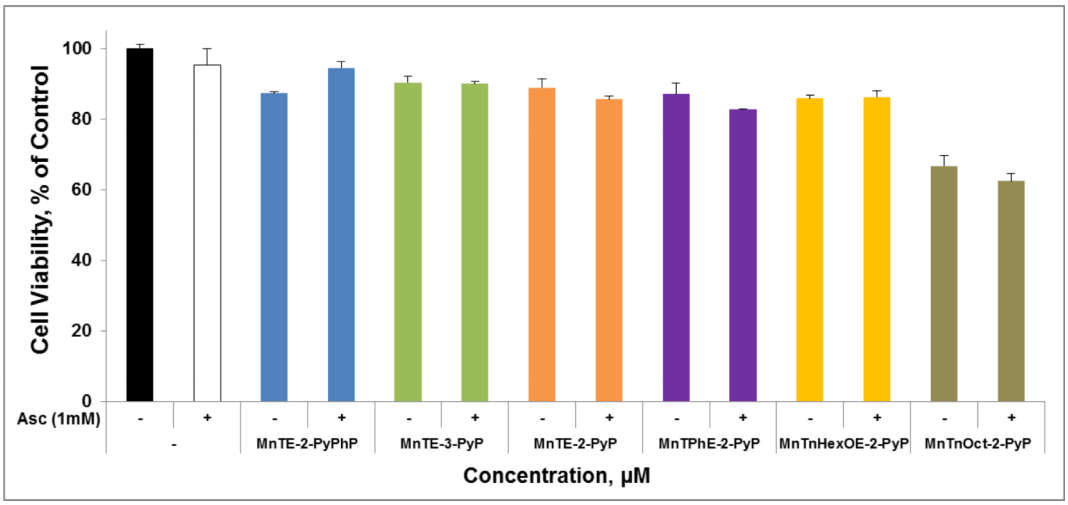

Figure 12. MnP/Asc system is not toxic to non-cancerous human epithelial breast HBL-100 cell line

Cells were incubated with MnP (10 μM) +/− ascorbate (1 mM) for 24 hours, followed by MTT-based assessment of cell viability.

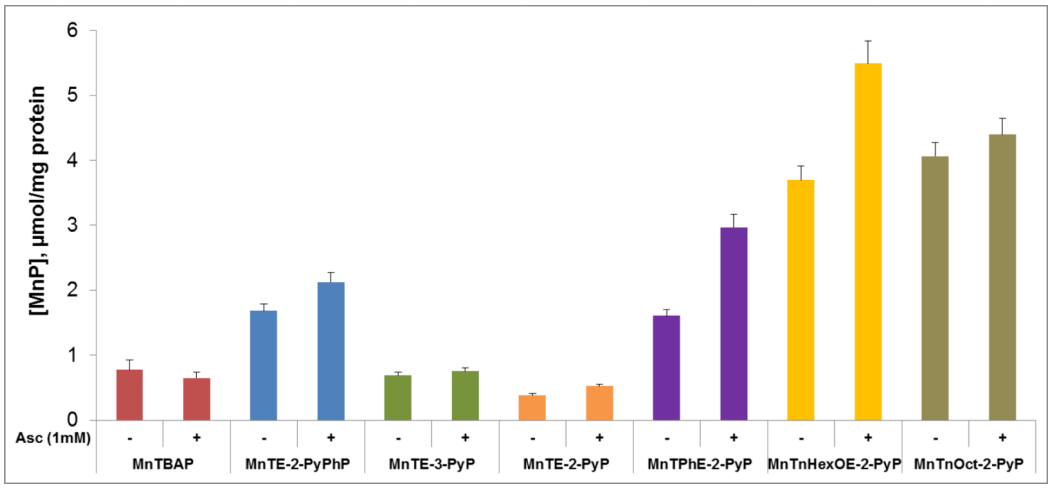

Figure 13. Cellular uptake of MnPs

4T1 cells were incubated with 5 μM MnP in the absence and presence of 1 mM ascorbate. Catalase (1000 unit/mL) was added to the medium to prevent cell damage by H_2O_2 produced *via* MnP/Asc coupling.

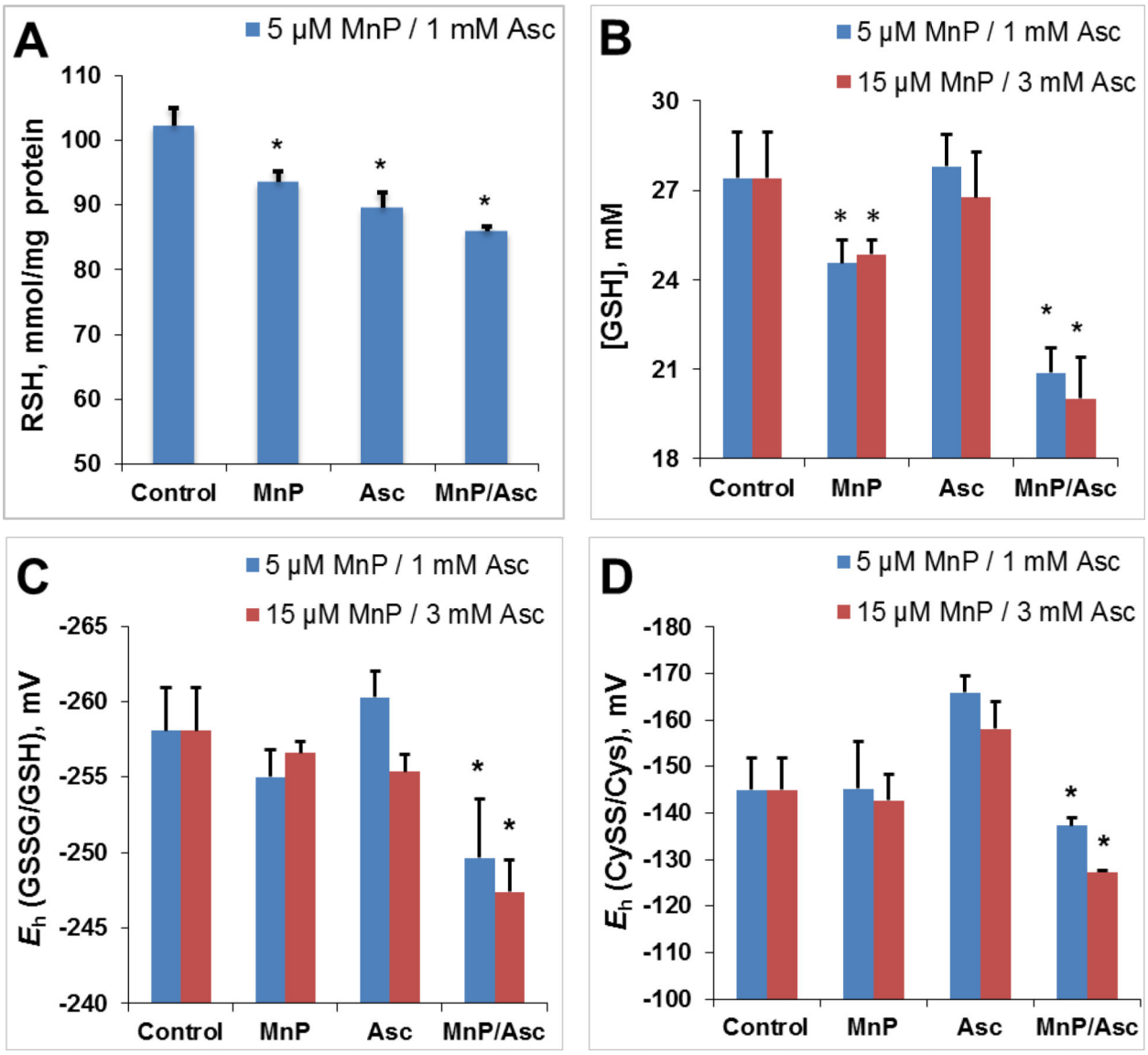

Figure 14. Effect of MnP/Asc treatment on intracellular thiol redox status

The 4T1 cells were treated for 4 hours with MnTE-2-PyP^{5+} (5 μM or 15 μM) or ascorbate (1 mM or 3 mM) alone or in combination. **(A)** Intracellular concentrations of reduced total thiols were measured spectrophotometrically in the cell lysates using 5,5'-dithiobis-(2-nitrobenzoic acid) (Ellman's reagent, DTNB). (**B**) Significant reduction of intracellular GSH concentration is observed in 4T1 cells as a result of MnP/Asc treatment. (**C**) Steady-state reduction potentials (E_h) were determined for intracellular GSSG/GSH redox couple in various treatment cohorts. (**D**) Steady-state cellular reduction potentials (E_h) were determined for intracellular CySS/Cys redox couple in various treatment cohorts. The E_h values were calculated using Nernst equation as described previously [62]. Bars represent the mean ± SEM (*p < 0.05).

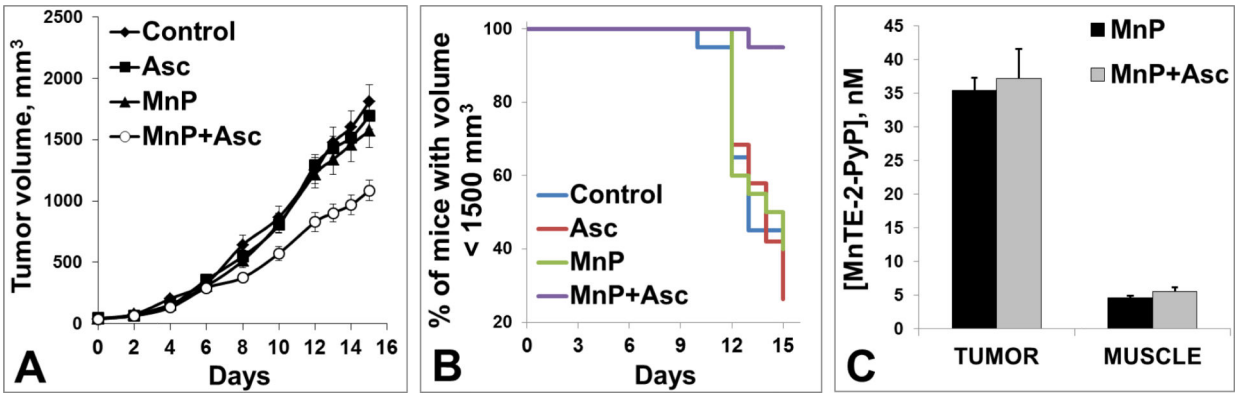

Figure 15.

(A) Anticancer effect of MnTE-2-PyP^{5+}/Asc on a growth of 4T1 mammary carcinoma in a mouse flank. 10^6 cells were implanted into the flank of Balb/c mouse. Treatment started 24 hours after the injection of 4T1 tumor cells. MnTE-2-PyP^{5+} was administered sc at 0.2 mg/kg/day and ascorbate was given ip at 4g/kg/day throughout the study. 20 mice were used per group. **(B)** At day 15th, 95% of mice treated with MnP/Asc have tumors whose volumes were less than 1,500 mm^3 **(C)** ~7-fold higher accumulation of MnTE-2-PyP^{5+} was found in tumor than in muscle and was not affected by ascorbate. Of note, a 2nd study was done where treatment started once tumors on average reached 80 mm^3. As similar tumor suppression was observed in either study, early start of treatment when tumor was not established has no additional impact on tumor growth suppression by MnP/Asc.

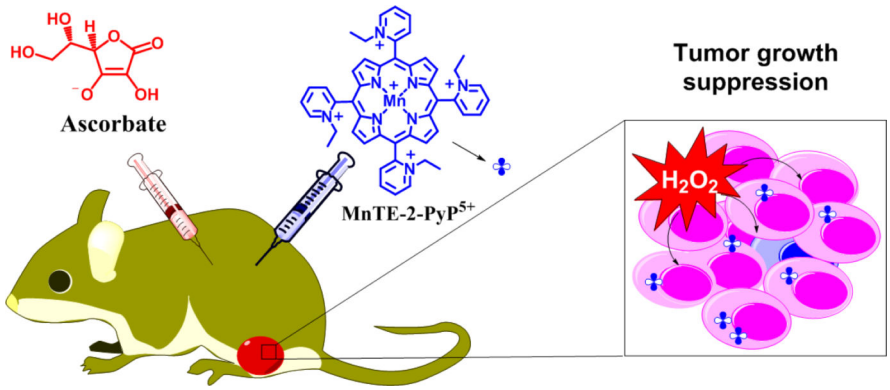

Figure 16. Cooperative actions of MnP/Asc/H_2O_2 system result in suppression of tumor growth

enhanced tumor H_2O_2 levels *via* MnP/Asc coupling, high rate of MnP-catalyzed ascorbate oxidation, increased tumor MnP and ascorbate accumulation and MnP/H_2O_2-driven oxidation of signaling proteins [8, 9].

Table 1

Spectrophotometrical and electrochemical characterization of MnP/Asc system.

MnPs	$E_{1/2}$, mV *vs* NHE	R_f	$v_0(Asc)_{ox}$, nM s^{-1}		$v_0(O_2)_{red}$, nM s^{-1}	
			Phosphate buffer	Tris buffer	Phosphate buffer	Tris buffer
$MnTBAP^{3-}$	−194	-	3.6±0.3	2.0±1.6	4.1±4.7	2.3±2.0
$MnTE\text{-}2\text{-}PyPhP^{5+}$	−65	0.28	49.6±8.7	70.8±7.5	15.2±2.8	11.8±1.4
$MnTE\text{-}3\text{-}PyP^{5+}$	+54	0.08	753.9±90.3	972.2±32.0	201.4±21.2	203.9±19.8
$MnTnHex\text{-}3\text{-}PyP^{5+}$	+66	0.50	639.2±7.2	864.5±41.1	193.1±40.2	191.7±10.8
$MnTE\text{-}4\text{-}PyP^{5+}$	+70	0.07	696.0±52.2	887.0±31.4	185.6±27.9	204.5±31.1
$MnTnOct\text{-}3\text{-}PyP^{5+}$	+74	0.55	838.0±7.1	993.6±10.0	225.4±44.5	216.5±20.0
$MnTnHex\text{-}4\text{-}PyP^{5+}$	+80	0.54	670.5±2.2	887.5±50.8	199.6±25.8	206.7±29.4
$MnTE\text{-}2\text{-}PyP^{5+}$	+228	0.06	679.5±28.0	922.0±89.6	285.7±37.1	307.7±35.1
$MnTPhE\text{-}2\text{-}PyP^{5+}$	+259	0.37	571.1±36.2	575.6±83.6	164.5±21.0	176.3±16.4
$MnTnBuOE\text{-}2\text{-}PyP^{5+}$	+277	0.43	474.1±26.3	856.9±21.0	159.8±28.9	256.5±45.7
$MnTnPen\text{-}2\text{-}PyP^{5+}$	+278	0.32	414.1±32.0	532.9±36.3	152.5±24.0	164.5±21.3
$MnTnHexOE\text{-}2\text{-}PyP^{5+}$	+313	0.50	226.9±5.0	469.7±78.7	81.3±14.3	135.6±10.2
$MnTnHex\text{-}2\text{-}PyP^{5+}$	+314	0.46	310.7±22.9	358.0±14.9	102.7±23.8	95.0±11.3
$MnTnOct\text{-}2\text{-}PyP^{5+}$	+367	0.49	306.3±65.3	304.4±36.8	74.5±15.5	72.1±6.9

Studies were carried out in 0.05 M Tris and potassium buffer, pH 7.8 at (25±1)°C. The metal-centered reduction potential for $Mn^{III}P/Mn^{II}P$ redox couple, $E_{1/2}$, the chromatographic parameter, R_f (compound path over solvent path on silica plates) as a measure of MnPs lipophilicity, initial rates of ascorbate oxidation ($v_0(Asc)_{ox}$ and initial rates of oxygen reduction, ($v_0(O_2)_{red}$.